Circuits and Systems
Mekelweg 4,
2628 CD Delft
The Netherlands
http://ens.ewi.tudelft.nl/

CAS-2019-4709373

M.Sc. Thesis

Identification of Quasi Normal Modes

Pranav Prakash
4709373

Abstract

Quasi-Normal Modes (QNMs) are a key concept in reduced-order models. In this thesis, we use Finite-Difference approach to create a discretized model of an open electromagnetic system in order to identify its QNMs and the Perfectly Matched Layer (PML) modes. We develop a structure of the QNMs and the PML modes and identify different regions of the eigenvalue distribution in our system. We validate the idea of dominant QNMs by using the identified QNMs to get the solution that was obtained using the Finite-Difference method.

Identification of Quasi Normal Modes
In Wave-Field Problems

This thesis is submitted in partial fulfillment of the
requirements for the degree of

Master of Science

in

Electrical Engineering

by

Pranav Prakash
born in Hazaribag, India

This work was performed in:

Circuits and Systems Group
Department of Microelectronics
Faculty of Electrical Engineering, Mathematics and Computer Science
Delft University of Technology

Delft University of Technology

Delft University of Technology
Department of
Microelectronics

The undersigned hereby certify that they have read and recommend to the Faculty of Electrical Engineering, Mathematics and Computer Science for acceptance of thesis entitled **"Identification of Quasi Normal Modes"** by **Pranav Prakash** in partial fulfillment of the requirements for the degree of **Master of Science**.

Dated: 19th of August, 2019

Chairman: _____
dr.ir. Rob F. Remis

Advisor: _____
dr.ir. Rob F. Remis

Committee Members: _____
dr.ir. Rob F. Remis

_____
dr. N. V. Budko

_____
dr. ir. J. T. Zimmerling

Preface

In this Master's thesis, we worked on identifying and clustering of eigenvalue distribution of an Electromagnetic system. This thesis has been submitted as a requirement for the fulfillment of Master of Science degree in Electrical Engineering at Delft Institute of Technology.

The research work was done under the supervision of dr.ir. R.F. Remis in the Circuits and Systems group at TU Delft. It goes without saying that without him, it would not have been possible to finish this thesis and for that, I would like to express my sincere gratitude for his guidance and support throughout my thesis. I thank him for motivating me and his valuable recommendations and suggestions on the report.

I would also like to thank my friends and family in helping me with my thesis report and brainstorming ideas.

Pranav Prakash
Delft, The Netherlands
19th of August, 2019

Contents

List of Figures

1 Introduction

Resonant systems are a class of system that are bounded on the spatial domain whose response has relative maxima for inputs of certain frequencies (natural frequencies of the system). When perturbed by one of these frequencies, the system oscillates in a motion given by its normal modes. A natural mode of a system is the pattern in which the entire resonating system oscillates. This pattern is defined by the geometry and the imposed boundary conditions on the system. Under the influence of input, the motion of the system is the superposition of its modes corresponding to the frequencies present in the input signal. However, these normal modes exist only for systems with a high Q factor (Quality factor of the resonator, higher Q factor means smaller damping [11]). Most of the practical systems in real life are leaky, which means that they continuously lose energy to infinity. The domain for such an open system extends to the whole universe and their modes are purely continuous [10]. The damping in these resonant systems can't be accurately modeled using the normal modes and therefore the concept of Quasi Normal Modes with complex frequencies is used [3]. These modes much like the normal modes depend upon the structure and the composition of the medium and not on the frequency of the input signal.

Certain classes of systems on reacting with light dissipate energy as oscillating electromagnetic (EM) waves. Nano-resonators are an example, where the use of a suitable input pulse can produce a resonant EM field. For these systems, it is important to find the right excitation frequency for the material in use. Once a proper frequency which is characterized by the intrinsic property of the material is found, an appropriate input signal can be used for the light-matter interaction [6]. These excitation frequencies are found by solving for eigenvalues of the Maxwell equations without any external source.

There are other problems in the domain of wave-field imaging, nano-optics, plasmon resonators, identification of resonant modes in nano-resonators, etc, that requires the solution of Maxwell equations in the respective media for different frequencies and parameters. For media with complex geometries, where it is not possible to get an analytical solution, the system is solved by using popular techniques such as Finite-Difference Time-Domain (FDTD), Finite Element Method (FEM), etc after discretizing it. The discretization is done on a nano-scale to accommodate for the Nyquist frequency which should ideally be more than double the bandwidth of the input pulse. The discretization process thus results in millions of data points which is difficult to handle even on a supercomputer. This calls for a more intelligent and robust way to handle this problem. If the QNMs of an open system are known, the evolution of EM waves generated by an input can be modeled as a linear combination of these QNMs instead of solving for the computationally intensive Maxwell's equations.

Another problem in working with such open systems is simulating them on a spatially-limited domain. Creating an artificial boundary results in outgoing waves getting reflected because such boundaries have the same effect as having a medium

with different properties than its surrounding. Therefore, certain mathematical tricks are employed to simulate such systems in a finite environment to generate the actual system output. One way to do that is by using a boundary layer called a Perfectly Matched Layer where the outgoing fields are damped. These methods and the discretization process will be discussed further in this report.

This thesis deals with wave-field problems in the nano-optics domain. These systems when discretized can produce system matrices in the order of several million and may take a considerable amount of time to solve through classical methods. In this respect, the resonant property of the systems can be exploited to develop smarter solutions which can drastically reduce the computational cost. It has been experimentally observed that QNMs can be used to accurately describe the output of a system and if known, can be used to construct the solution without solving Maxwell equations [8]. Another important result from these experiments is that only a few dominant QNMs are sufficient to trace the actual response of the system for a wide range of frequencies.

Several experiments have been performed over time to verify this result. C. Sauvan in his paper on "Theory of the Spontaneous Optical Emission of Nanosize Photonic and Plasmonic Resonators" [9] concluded that the spontaneous decay rate for a single gold nano-rod calculated using numerical data was approximated by a single QNM to an excellent degree. The experiment was further verified by using a more complex system of two gold nano-rods placed close to each other. The decay rate calculated using numerical data was found to agree with what was calculated using the sum of responses of the QNM of each of the nano-rods considered independently. In another paper by Remi Faggiani on modal analysis [6], it was concluded that the temporal response of the scattered wave in a gold nano-rod could be approximated using a single dominant QNM and an even higher degree of agreement could be found with the experimental data using three dominant QNMs.

The focus of the project will be to find these QNMs, separate them from the Perfectly Matched Layer (PML) modes, to study and possibly obtain a structure of these modes. The analysis can help speed up the calculation of eigenmodes for a more complex system. These modes are calculated in a Krylov subspace for larger systems like the one discussed in this thesis for computational efficiency. Previous works in this domain were heavily focused on Polynomial Krylov Subspace (PKS) and Extended Krylov Subspace (EKS) [4] because of the fewer computation requirement. Another method which is of interest regarding this thesis is the Rational Krylov Subspace (RKS). It is generally computationally more intensive than the other two because, while PKS and EKS converge to eigenvalues iteratively starting from the largest eigenvalue, RKS attempts to converge to several eigenvalues simultaneously around a region of chosen shifts by inverting the system matrix [13]. This means that if the shifted points are close to the actual eigenvalues of the matrix, RKS will converge much faster than the other two methods (PKS and EKS). Therefore, an advantage of RKS process concerning the result of this thesis is that once there is a suitable method to identify the QNMs, the RKS method can be used to converge to such modes efficiently by choosing appropriate shifts.

This report is structured into five chapters. It begins by developing a geometrically simple one-dimensional slab system which will be used throughout the report. In the

first chapter, we obtain the true scattering poles of the system through continuous analysis of Maxwell's equation, which governs the behavior of electromagnetic waves. Thereafter, a normalized discrete model for the same system is developed in chapter 3. Since the discretized system is to be simulated as an open system, the model is stretched to infinity using a PML in chapter 4. Then, the report finishes with experiment results and conclusion on the Quasi-Normal Modes of the discretized system in the next two chapters.

2 Continuous Analysis

2.1 Introduction

This chapter begins by developing a notion of Maxwell equations in a continuous space and time domain which governs the behavior of Electromagnetic (EM) fields. These equations will be used to solve for electric and magnetic fields in a geometrically simple system which will be used for further analysis in the report in subsequent chapters. In section 2.2.2, we calculate the scattering poles of the system. In this way, we develop a ground truth using an open system against which the results of the discrete model can be compared for validation in later stages.

2.2 Slab System

In this section, we introduce a system consisting of a slab-like medium to begin studying the modes of an EM system. Before coming to the slab system, we will introduce the Maxwell equations which are

$$-\nabla \times \mathcal{H} + \sigma\mathcal{E} + \epsilon\delta_t\mathcal{E} = -\mathcal{J}^{ext} \tag{2.1}$$

and

$$\nabla \times \mathcal{E} + \mu\delta_t\mathcal{H} = -\mathcal{K}^{ext}, \tag{2.2}$$

where $\mathcal{E}$ and $\mathcal{H}$ are the electric and the magnetic field vectors. The time varying $\mathcal{J}^{ext}$ and $\mathcal{K}^{ext}$ are the external electric and magnetic current density respectively and σ is the electrical conductivity, which depends on the medium. ϵ and μ are the electric permittivity and magnetic permeability which are also dependent on the material properties of the medium. These equations along with the imposed boundary conditions govern the evolution of field quantities $\mathcal{E}(x,t)$ and $\mathcal{H}(x,t)$ with space and time.

Now that the notion of Maxwell equations has been established, we can proceed to model a system with a source where we can study the evolution of field quantities $\mathcal{E}$ and $\mathcal{H}$ in space for different frequencies. The experiment is based on a slab system which has a certain permittivity profile (a constant > 1 in the simplest case). A sketch of the system is shown in figure 2.1.

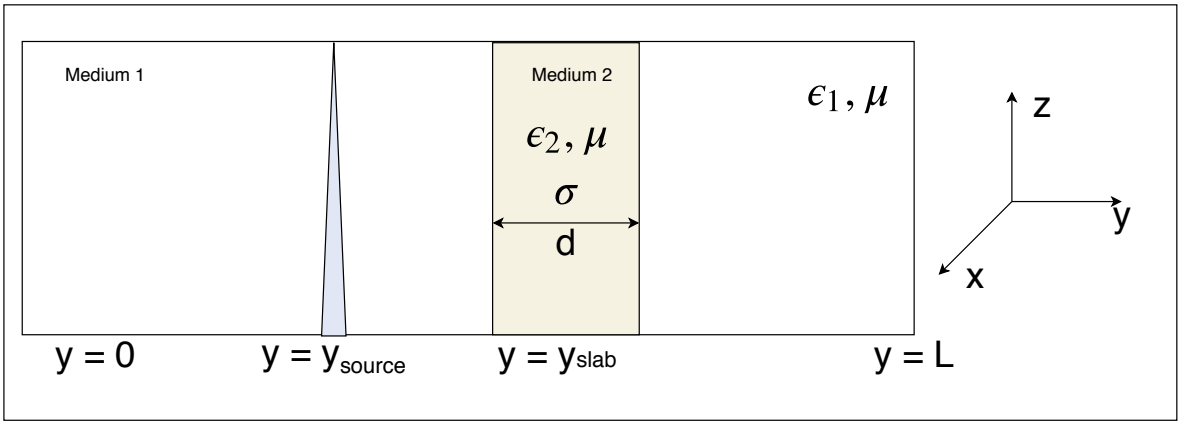

Figure 2.1: The slab system

The rectangular region is a slab of a constant permittivity surrounded by the vacuum of permittivity one shown as the region of white space. A Gaussian pulse is generated at a certain distance from the slab shown as the triangular region. The slab is of width d and the medium has a permittivity ϵ_2 and electrical conductivity σ. Both the regions have a magnetic permeability μ. The advantage of this configuration is that the problem can be modeled using Maxwell's equations and that an analytical solution can be computed as discussed below.

In the one-dimensional system, the waves are propagating in y direction with the source pointing in the z direction. The direction constraint implies that $\partial_z = \partial_x = 0$ in the Maxwell's equations. Furthermore, the electric field will be oscillating in z direction because the source is pointing in that direction. Using the above results in equation 2.1 and 2.2, we are left with only $\mathcal{E}_z$ and $\mathcal{H}_x$ term that are non-zero. Accounting for the directions of other field quantities, magnetic field density $\mathcal{K}$ for the given one-dimensional problem is chosen to be pointing in the x direction. Now, the one-dimensional Maxwell wave equations are given by:

$$\partial_y \mathcal{H}_x + \sigma \mathcal{E}_z + \epsilon_r \partial_t \mathcal{E}_z = -\mathcal{J}_z^{ext} \tag{2.3}$$

and

$$\partial_y \mathcal{E}_z + \mu_r \partial_t \mathcal{H}_x = -\mathcal{K}_x^{ext} \tag{2.4}$$

2.2.1 Analytical Equation

The analytical solution of the slab system can be calculated by solving for equation 2.3 and 2.4 along with the boundary conditions on the medium boundary. The electric field in such a system so obtained is given below [12]:

$$E_{medium} = e_i \times \left(A^+ e^{-\gamma_2 (x - x_{source})} + A^- e^{\gamma_2 (x - x_{source})} \right)$$

$$E_{reflected} = R e_i e^{\gamma_1 (x - x_{source})}$$

$$E_{transmitted} = Te_i e^{-\gamma_1 * (x - x_{source})}$$

where e_i is the field due to the source at any chosen origin. A^+ and A^- depend on the permittivity of the medium and the surrounding, R is the reflection coefficient and T is the transmission coefficient and are given by:

$$A^+ = \frac{\frac{2Y_1}{Y_1+Y_2}}{1 - \left(\frac{Y_1-Y_2}{Y_1+Y_2}\right)^2 e^{-2\gamma_2 d}},$$

$$A^- = \frac{\frac{-2Y_1(Y_1-Y_2)}{(Y_1+Y_2)^2} e^{-2\gamma_2 d}}{1 - \left(\frac{Y_1-Y_2}{Y_1+Y_2}\right)^2 e^{-2\gamma_2 d}},$$

$$R = \frac{\frac{Y_1-Y_2}{Y_1+Y_2}(1 - e^{-2\gamma_2 d})}{1 - \left(\frac{Y_1-Y_2}{Y_1+Y_2}\right)^2 e^{-2\gamma_2 d}}$$

and

$$T = \frac{\frac{4Y_1Y_2}{(Y_1+Y_2)^2} e^{(\gamma_1-\gamma_2)d}}{1 - \left(\frac{Y_1-Y_2}{Y_1+Y_2}\right)^2 e^{-2\gamma_2 d}},$$

where Y_1 and Y_2 are the electrical admittance in the open region(1) and and the slab region(2) respectively given by:

$$Y_1 = \sqrt{\frac{\epsilon_1}{\mu}}$$

and

$$Y_2 = \left(\frac{\sigma + s\epsilon_2}{s\mu}\right)^{\frac{1}{2}}$$

The quantities $\gamma_1 = s\sqrt{\epsilon_1\mu}$ and $\gamma_2 = [(\sigma + s\epsilon_2)s\mu)]$ are the propagation coefficients in the respective medium (vacuum and slab).

2.2.2 Scattering Poles

Looking at the denominator of reflection, transmission, A^+ and A^- coefficients, it is seen that the values blow up when $\left(\frac{Y_1-Y_2}{Y_1+Y_2}\right)^2 e^{-2\gamma_2 d} = 1$. The complex frequencies at which the equation is satisfied are termed as the scattering poles [5]. It is at these poles that the resonance occurs and the inputs at these frequencies will dominate the behavior of the system. The scattering poles can be calculated analytically for the system in which the slab has $\sigma = 0$ because it allows the square term $\left(\frac{Y_1-Y_2}{Y_1+Y_2}\right)^2$ to be independent of s. If $\sigma \neq 0$, the unknown term s is present in both the exponential and the square term and the problem will then require a non-linear solver to obtain the poles. To obtain the poles for $\sigma = 0$, let $\left(\frac{Y_1-Y_2}{Y_1+Y_2}\right)^2 = K$.
Then the scattering poles are given by:

$$Ke^{-2\gamma_2 d} = 1,$$

which gives

$$s = \frac{\ln \mathrm{K}}{\phi} + j\frac{2n\pi}{\phi}, \text{ for n} = 0,\ 1,\ 2, \cdots$$

where we have taken $\phi = 2\sqrt{\epsilon_2}c^{-1}d$ and $c = \frac{1}{\sqrt{\epsilon_o \mu_o}}$.
The scattering poles are therefore located parallel to the imaginary axis.

With this result, we have found the solution for wave-field inside an open system and established an idea of the nature of its scattering poles which were found to be countably infinite. This result will later be used to draw a comparison with the eigenvalues of the Finite-Difference model of the slab system in subsequent chapters.

3 Discrete Model

In this chapter, we create a discretized model of the slab system used in the previous chapter. We start with the normalization of the field quantities so that they are in the same scale and the numerical stability is maintained. The slab system described previously is an open system. For simulation purposes, we truncate the system with a Perfectly Electrically Conducting (PEC) boundary conditions following which the system is discretized in the spatial domain. Finally, the chapter concludes with discussions on the properties of the discretized equations.

3.1 Normalization

For the normalization of the field quantities, we begin with general Maxwell equations which are:

$$\begin{aligned} -\nabla \times \mathcal{H} + \sigma\mathcal{E} + \epsilon\delta_t\mathcal{E} &= -\mathcal{J}^{ext} \\ \nabla \times \mathcal{E} + \mu\delta_t\mathcal{H} &= -\mathcal{K}^{ext} \end{aligned}$$

The field quantities, the external inputs and the medium parameters have been introduced in the previous chapter and therefore, we begin directly with normalization process by scaling the following quantities:

$$\boxed{y \to Ly' \ \text{ and } \ t \to c_o^{-1}Lt'}, \tag{3.1}$$

where L is the length of the truncated space around the slab that will be used in the simulation and $c_o = 3 \times 10^8$ is the speed of light in vacuum. The normalized spatial scale, therefore ranges from $y' = 0$ to 1. Now, substituting the equation with the scaled variables gives

$$\begin{aligned} -L^{-1}\nabla' \times \mathcal{H}(Ly', c_o^{-1}Lt') + \sigma(Ly')\mathcal{E}(Ly', c_o^{-1}Lt') + \epsilon c_o L^{-1}\delta_{t'}\mathcal{E}(Ly', c_o^{-1}Lt') = \\ -\mathcal{J}^{ext}(Lx', c_o^{-1}Lt') \end{aligned}$$

$$\implies L^{-1}\nabla' \times E(Ly', c_o^{-1}Lt') + \mu_r\mu_o c_o L^{-1}\delta_{t'}\mathcal{H}(Ly', c_o^{-1}Lt') = -\mathcal{K}^{ext}(Ly', c_o^{-1}Lt')$$

In obtaining the above equations, we have used the relations $\epsilon = \epsilon_r\epsilon_o$, $\mu = \mu_r\mu_o$ and $c_o = \frac{1}{\sqrt{\mu_o\epsilon_o}}$. Multiplying the equation throughout with L, it is obtained that:

$$\begin{aligned} Z_o\nabla' \times \mathcal{H} + Z_oL\sigma E' + \epsilon_r\delta_{t'}\mathcal{E} &= -Z_oL\mathcal{J}^{ext} \\ \nabla' \times \mathcal{E} + \mu_r' Z_o\delta_{t'}\mathcal{H} &= -L\mathcal{K}^{ext}, \end{aligned}$$

where $Z_o = \sqrt{\frac{\mu_o}{\epsilon_o}}$ is the electrical impedance. The normalized Maxwell equations thus obtained can be written as:

$$\nabla' \times \mathcal{H}' + \sigma' \mathcal{E}' + \epsilon_r \delta_{t'} \mathcal{E}' = -\mathcal{J}^{ext\prime}$$
$$\nabla' \times \mathcal{E}' + \mu_r \delta_{t'} \mathcal{H}' = -\mathcal{K}^{ext\prime},$$

where the field quantities on the normalized scale are related to the actual field values through the following equations:

$$\mathcal{E}' = \mathcal{E}(Ly', c_o^{-1} Lt'),$$
$$\mathcal{H}' = Z_o \mathcal{H}(Ly', c_o^{-1} Lt',$$
$$\sigma' = L Z_o \sigma(LX'),$$
$$\mathcal{J}^{ext\prime} = L Z_o \mathcal{J}^{ext}(Ly', c_o^{-1} Lt'),$$

and

$$\mathcal{K}^{ext\prime} = L\mathcal{K}^{ext}(Ly', c_o^{-1} Lt')$$

From here onwards, the normalized field quantities will be used without the prime symbol and unless specified otherwise, all the values are on the scaled time and distance.

3.2 Discretization

The slab system described in chapter 2 is truncated with a PEC boundary condition as shown in figure 3.2. To make the finite domain model simulation-ready, it is discretized on a primary and a dual grid. Electric fields are calculated on the primary grid and magnetic field on the dual grid. The discretized equation so obtained is put in the form of a state-space equation as described below.

For the one dimensional case, if the current source is in the z direction, only the fields E_z and H_x are non zero and the wave travels in the y direction. Therefore, the one dimensional Maxwell equations for a lossy medium are:

$$\partial_y \mathcal{H}_x + \sigma \mathcal{E}_z + \epsilon_r \partial_t \mathcal{E}_z = -\mathcal{J}_z^{ext} \tag{3.2}$$
$$\partial_y \mathcal{E}_z + \mu_r \partial_t \mathcal{H}_x = -\mathcal{K}_x^{ext} \tag{3.3}$$

The above equations can be written in the compact form as:

$$(D + S + M\partial_t) f = -q$$

where the medium matrices are

$$D = \begin{bmatrix} 0 & \partial_y \\ \partial_y & 0 \end{bmatrix}, \; S = \begin{bmatrix} \sigma & 0 \\ 0 & 0 \end{bmatrix} \text{ and } M = \begin{bmatrix} \epsilon_r & 0 \\ 0 & \mu_r \end{bmatrix}$$

and the field and source vectors are:

$$\mathbf{f} = \begin{bmatrix} \mathcal{E}_z \\ \mathcal{H}_x \end{bmatrix} \text{ and } \mathbf{q} = \begin{bmatrix} \mathcal{J}_z^{ext} \\ \mathcal{K}_x^{ext} \end{bmatrix}$$

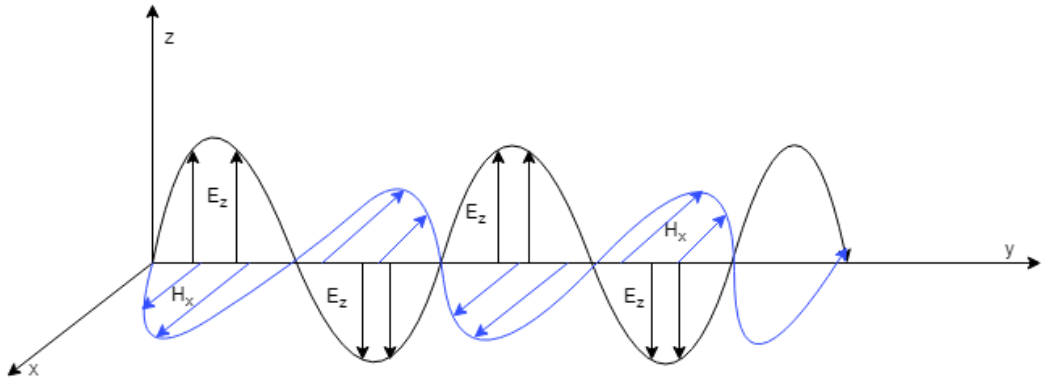

Figure 3.1: Electric and Magnetic field in a one-dimensional slab and the chosen directions

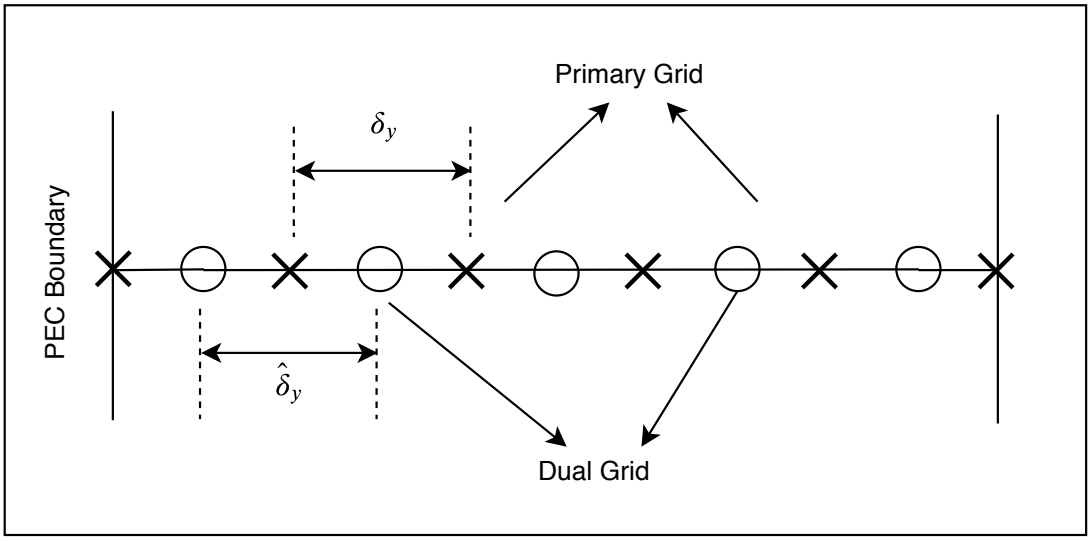

Figure 3.2: Primary(o) and dual (×) nodes on the uniform grid (adapted from *Laboratory of Electromagnetic Research* by Rob F. Remis)

For the discretization of the fields, a primary and dual grid is assumed on the y axis as shown in figure 3.2. The primary grid is defined as:

$$\Omega_y^p = \{y_q,\ q = 0, 1, ...Q+1,\ y_0 = 0,\ y_{Q+1} = l_y\}$$

and the corresponding step sizes are

$$\delta_{y;q} = y_q - y_{q-1} \text{ for } q = 1, 2, ..., Q+1$$

The dual grid is defined as:

$$\Omega_y^d = \{\hat{y}_1, q = 1, 2, ...Q+1, 0 < \hat{y}_q < l_y\}$$

and the corresponding step sizes are:

$$\hat{\delta}_{y;q} = \hat{y}_{q+1} - \hat{y}_1 \text{ for } q = 1, 2, ..., Q$$

Maxwell's equations on the discrete system are, therefore:

$$\delta_y H_x|_{y=y_q} + \sigma(y_q)\mathcal{E}_z(y_q,t) + \epsilon_r(y_q)\partial_t\mathcal{E}_z(y_q,t) = -\mathcal{J}_z^{ext}(y_q,t)$$

for $q = 1, 2, ..., Q$ and,

$$\delta_y \mathcal{E}_z|_{y=\hat{y_q}} + \mu(\hat{y}_q)\partial\mathcal{H}(\hat{y}_q,t) = -\mathcal{K}_x^{ext}(\hat{y}_q,t)$$

for $q = 1, 2, ..., Q+1$.

The spatial differentiation is discretized on one dimension using the following approximation:

$$\delta_y H_x|_{y=y_q} = \frac{H_x(\hat{y}_{q+1},t) - H_x(\hat{y}_q,t)}{\hat{\delta}_{y;q}} + \xi(y_q)$$

and

$$\delta_y \mathcal{E}_z|_{y=\hat{y_q}} = \frac{\mathcal{E}_z(y_q,t) - \mathcal{E}_z(y_{q-1},t)}{\delta_{y;q}} + \xi(y_{\hat{q}})$$

where $\xi(y)$ is the error due to discretization at a point y.

Electric field $\mathcal{E}_z$ and magnetic field $\mathcal{H}_x$ is discretized on the primary and the dual grid respectively as follows:

$$\mathbf{e_z} = [\mathbf{e_z}(y_1,t), \mathbf{e_z}(y_2,t), ..., \mathbf{e_z}(y_Q,t)]^\intercal$$

and

$$\mathbf{h_x} = [\mathbf{h_x}(\hat{y}_1,t), \mathbf{h_x}(\hat{y}_2,t), ..., \mathbf{h_x}(\hat{y}_{Q+1},t)]^\intercal$$

which are the finite domain approximations of the fields at points on the discrete domain. Also, the Perfectly Conducting boundary condition means that on the primary grid, $e_z(y_0,t) = e_z(y_{Q+1},t) = 0$.

Now, writing Maxwell's equation for some of the points on the discrete scale, it is obtained that:

$$\begin{aligned}
y_{q=1} \ |; \ & \frac{\mathbf{h_x}(\hat{y}_2,t) - \mathbf{h_x}(\hat{y}_1,t)}{\hat{\delta}_1} + \sigma(y_1)\mathbf{e_z}(y_1,t) + \epsilon_r(y_1)\partial_t\mathbf{e_z}(y_1,t) = -j_z^{ext}(y_1,t) \\
y_{q=2} \ |; \ & \frac{\mathbf{h_x}(\hat{y}_3,t) - \mathbf{h_x}(\hat{y}_2,t)}{\hat{\delta}_2} + \sigma(y_2)\mathbf{e_z}(y_2,t) + \epsilon_r(y_2)\partial_t\mathbf{e_z}(y_2,t) = -j_z^{ext}(y_2,t) \\
& \vdots \\
y_{q=Q} \ |; \ & \frac{\mathbf{h_x}(\hat{y}_{Q+1},t) - \mathbf{h_x}(\hat{y}_Q,t)}{\hat{\delta}_Q} + \sigma(y_Q)\mathbf{e_z}(y_Q,t) + \epsilon_r(y_Q)\partial_t\mathbf{e_z}(y_Q,t) = -j_z^{ext}(y_Q,t)
\end{aligned}$$

and

$$\begin{aligned}
\hat{y}_{q=1} \;|;\; \frac{\mathbf{e_z}(y_1,t)-0}{\delta_1} + \mu_r(\hat{y}_1)\partial_t \mathbf{h_x}(\hat{y}_1,t) &= -k_x^{ext}(\hat{y}_1,t)\\
\hat{y}_{q=2} \;|;\; \frac{\mathbf{e_z}(y_2,t)-\mathbf{e_z}(y_1,t)}{\delta_2} + \mu_r(\hat{y}_2)\partial_t \mathbf{h_x}(\hat{y}_2,t) &= -k_x^{ext}(\hat{y}_2,t)\\
\vdots&\\
\hat{y}_{q=Q+1} \;|;\; \frac{0-\mathbf{e_z}(y_Q,t)}{\delta_Q} + \mu_r(\hat{y}_Q)\partial_t \mathbf{h_x}(\hat{y}_Q,t) &= -k_x^{ext}(\hat{y}_Q,t)
\end{aligned}$$

Using the above approximation for discretized differentiation and the boundary conditions, the differentiation operator on the primary and dual grid is given by:

$$\hat{Y} = \begin{bmatrix}
-\hat{\delta}_{y:1}^{-1} & \hat{\delta}_{y:1}^{-1} & & & & \\
 & -\hat{\delta}_{y:2}^{-1} & \hat{\delta}_{y:2}^{-1} & & & \\
 & & & \cdots & & \\
 & & & & \cdots & \\
 & & & & -\hat{\delta}_{y:Q}^{-1} & \hat{\delta}_{y:Q}^{-1}
\end{bmatrix}$$

$$Y = \begin{bmatrix}
\delta_{y:1}^{-1} & & & & & \\
-\delta_{y:2}^{-1} & \delta_{y:2}^{-1} & & & & \\
 & -\delta_{y:3}^{-1} & \delta_{y:3}^{-1} & & & \\
 & & & \cdots & & \\
 & & & & \cdots & \\
 & & & & -\delta_{y:Q}^{-1} & \delta_{y:Q}^{-1} \\
 & & & & & -\delta_{y:Q+1}^{-1}
\end{bmatrix}$$

The discrete Maxwell equations are now given by:

$$\begin{aligned}
\hat{Y}h_x + M_\sigma \mathbf{e_z} + M_\epsilon \partial_t \mathbf{e_z} &= -j_z^{ext}\\
Y\mathbf{e_z} + M_\mu \partial_t \mathbf{h_x} &= -k_z^{ext}
\end{aligned}$$

and the compact form is now given by:

$$(D+S+Ms)\mathbf{f} = -\mathbf{q},$$

where

$$D = \begin{bmatrix} 0 & \hat{Y} \\ Y & 0 \end{bmatrix},\; S = \begin{bmatrix} M_\sigma & 0 \\ 0 & 0 \end{bmatrix} \text{ and } M = \begin{bmatrix} \epsilon_r & 0 \\ 0 & \mu_r \end{bmatrix}$$

and all the variables are in the Laplace domain. On multiplying the whole equation by M^{-1}, it is obtained that:

$$(A+sI)\mathbf{f} = -\mathbf{b},$$

where, $A = M^{-1}(D+S)$ and $b = M^{-1}\mathbf{q}$. This form will now be used for further computations. Here, b acts as the source. It can also be shown that A is skew-symmetric

in the inner-product sense for a lossless system ($S = 0$) in free space ($M = I$) in the case of which $A = D$.

The first step is observing that the differentiation matrix Y and $\hat{Y}$ can be re-written as a product of two matrices by introducing the step-size matrix and a bi-diagonal matrix B.

The step size matrices are:

$$\hat{W}_y = \begin{bmatrix} \hat{\delta}_{y;1} & 0 & 0 & \cdots & 0 \\ 0 & \hat{\delta}_{y;2} & 0 & \cdots & 0 \\ 0 & 0 & \hat{\delta}_{y;3} & \cdots & 0 \\ \vdots & & \vdots & \ddots & \vdots \\ 0 & 0 & 0 & \cdots & \hat{\delta}_{y;Q} \end{bmatrix} \text{ and } W_y = \begin{bmatrix} \delta_{y;1} & 0 & 0 & \cdots & 0 \\ 0 & \delta_{y;2} & 0 & \cdots & 0 \\ 0 & 0 & \delta_{y;3} & \cdots & 0 \\ \vdots & & \vdots & \ddots & \vdots \\ 0 & 0 & 0 & \cdots & \delta_{y;Q+1} \end{bmatrix}$$

The bi-diagonal matrix $\mathcal{B}_Q$ is Q by $Q+1$ matrix with all the diagonal entries as -1 and the upper diagonal entries as 1. For example, a

$$\mathcal{B}_3 = \begin{bmatrix} -1 & 1 & 0 & 0 \\ 0 & -1 & 1 & 0 \\ 0 & 0 & -1 & 1 \end{bmatrix}$$

Now, the differentiation matrix Y and $\hat{Y}$ can be easily written as:

$$\hat{Y} = \hat{W}_y^{-1}\mathcal{B}_Q \text{ and } Y = -W_y^{-1}\mathcal{B}_Q^\intercal$$

Pre-multiplying both the expressions by $\hat{W}_y^{-1}$ and W_y^{-1} respectively and taking transpose of the first expression and using the fact that the step-size matrices are the symmetric, diagonal matrices, it is obtained that:

$$(\hat{W}_y\hat{Y})^\intercal = \mathcal{B}_Q^\intercal \text{ and } -(W_yY) = \mathcal{B}_Q^\intercal$$

Thus, $\hat{Y}^\intercal\hat{W}_y = -W_yY$. To extend this symmetry property to the matrix D and in turn to the matrix A, following matrix is constructed,

$$W = \begin{bmatrix} \hat{W}_y & 0 \\ 0 & W_y \end{bmatrix}$$

Using the result that $\hat{Y}^\intercal\hat{W}_y = -W_yY$ along with matrix W, it can be seen that:

$$D^\intercal W = -WD$$

which makes D a skew symmetrix matrix which has all imaginary eigenvalues and also follows the law of conservation of energy [7]. Thus the field value obtained from using only the D operator are purely oscillatory in nature without any decay. Adding loss S shifts the eigenvalues away from the imaginary axis in a region of damping.

4 Perfectly Matched Layer

4.1 Introduction

In our approach to create the discretized equation for an open system, we have so far obtained a model on a finite domain with Perfectly Electrically Conducting (PEC) boundary conditions. However, there is an inherent problem with the model because of the truncation of the open domain with PEC conditions, which results in outgoing waves getting reflected from the boundary. This is unlike the open system that was discussed in chapter 2, where the waves propagate to infinity. This chapter addresses the issue by implementing an absorbing layer at the boundary which attenuates the outgoing waves with minimal reflections. The chapter begins with a brief introduction to Perfectly Matched Layer (PML) and its history along with the mathematical definition following which it is applied to the Maxwell equations. Finally, the modified Maxwell equations are discretized to provide us with a model whose behavior is similar to the open slab system from chapter 2.

4.2 PML

Initially, the reflections were avoided by putting an absorbing boundary condition by simply making the reflection coefficient zero for the normally incident waves. This method was later on improved by using an absorbing layer occupying a portion of the simulation volume to absorb the outgoing waves. However, this method was dependent on the angle and the frequency of the wave hitting the layer. The reflections could only be avoided for waves hitting the boundary at certain angles until Berenger came up with a better technique of using PML, which was independent of the incident angle [1]. Berenger's PML was later extended to 3-dimensions by introducing the stretched-coordinate approach [2]. The idea behind the approach is to introduce loss in the region near the boundary by extending the space outside the region of interest in the complex domain [7].
In this paper, we use a stretched-coordinate PML function as the absorbing layer. In the PML layer, the waves propagating in y direction is continued to the complex domain via a stretching function to introduce attenuation. The stretching function used here is:

$$\mathcal{X}_y(y,s) = K_y(y) + \frac{\zeta_y(y)}{s} \tag{4.1}$$

where,

$$K_y(y) = 1;\ \zeta_y(y) = 0$$

for $x \in (d_x, l_x - d_x)$ (inside the target region) and

$$K_y(y) = 1; \quad \zeta(y) = \alpha y^2 \tag{4.2}$$

for $y \in$ PML region. The attenuation function $\zeta(y) = \alpha y^2$ is chosen to be quadratic to provide a smooth transition from the medium to the PML, thus keeping the reflection due to a change in boundary to a minimum. The strength of PML depends upon the magnitude of $\mathcal{X}_y(y, s)$ in the PML area and the PML length d_x. If the PML is required to be of small length, then α needs to be high to cause rapid exponential decay. However, using a high magnitude for α in a small PML area can cause numerical reflections due to discretization and reflections due to a rapid change in the boundary. Therefore, a suitable value needs to be chosen for the PML length d_x and the PML constant α [7].

4.2.1 Modified Maxwell equations

The stretching function is applied to the differential operator in the spatial domain at the boundary area, which results in dampening of the fields in that region, making it seem like that the boundaries have been stretched to infinity:

$$\mathcal{X}_y^{-1}\partial_y \mathcal{E}_z + s\mu_r \mathcal{H}_x = -\mathcal{K}_x^{ext} \tag{4.3}$$

and

$$\mathcal{X}_y^{-1}\partial_y \mathcal{H}_x + \sigma \mathcal{E}_z + s\epsilon_r \mathcal{E}_z = -\mathcal{J}_z^{ext}, \tag{4.4}$$

where $\mathcal{X}_x(x, s)$ is called the stretching function and is defined in equations 4.1 and 4.2.

To make the differential operator independent of the stretching function, the modified equations are multiplied throughout with $\mathcal{X}_y^{-1}$ to get the following set of modified Maxwell equations:

$$\partial_y \mathcal{E}_z + \mathcal{X}_y s\mu_r \mathcal{H}_x = -\mathcal{X}_y \mathcal{K}_x^{ext}$$

and

$$\partial_y \mathcal{H}_x + \mathcal{X}_y \sigma \mathcal{E}_z + \mathcal{X}_y s\epsilon_r \mathcal{E}_z = -\mathcal{X}_y \mathcal{J}_z^{ext}$$

Now, since the sources $\mathcal{K}_x$ and $\mathcal{J}_z$ lie outside the PML area

$$\mathcal{X}_y \mathcal{J}_z^{ext} = \mathcal{J}_z^{ext}$$

and

$$\mathcal{X}_y^{-1} \mathcal{K}_x^{ext} = \mathcal{K}_x^{ext}$$

Also, for the terms involving electric permittivity and magnetic permeability (last term on the left hand side of both the equations), the expressions can be modified to make the equations linear in s by multiplying it with the PML function $\mathcal{X}$:

$$\mathcal{X}_y s\mu_r \mathcal{H}_x = s\left(1 + \frac{\zeta_y(y)}{s}\right)\mu_r \mathcal{H}_x = \zeta_y(y)\mu_r \mathcal{H}_x + s\mu_r \mathcal{H}_x$$

$$\mathcal{X}_y s\epsilon_r \xi_z = s\left(1 + \frac{\zeta_y(y)}{s}\right)\epsilon_r \mathcal{E}_z = \zeta_y(y)\epsilon_r \xi_z + s\epsilon_r \xi_z$$

However, the same method cannot be applied to the current density term $\mathcal{X}_y \sigma \mathcal{E}_z$, because the non-linear term $\frac{1}{s}$ in the PML function doesn't cancel out after the multiplication as seen below:

$$\left(1 + \frac{\zeta_y(y)}{s}\right) \sigma \mathcal{E}_z = \sigma \mathcal{E}_z + \frac{\zeta_y(y)}{s} \sigma \mathcal{E}_z \tag{4.5}$$

To account for the nonlinear $\frac{1}{s}$ term in equation 4.5, we draw up two scenarios:

- **Scenario 1**: The slab is inside a lossy medium whose area is larger than the simulation domain of length L and the PML region has $\sigma \neq 0$
- **Scenario 2:** The simulation setting extends till vacuum. In this way, PML is set up in a region where $\sigma = 0$.

Modeling the Maxwell equations in scenario one is more difficult than the second one because of the non-linearity in s. In such a case, to eliminate the $\frac{1}{s}$ dependence of the equation in the term $\frac{\zeta_x(x)}{s} \sigma \mathcal{E}_z$, a new state $\mathcal{U}_z$ is introduced so that

$$\begin{aligned} \mathcal{U}_z &= \frac{\zeta_x(x)}{s} \sigma \mathcal{E}_z \\ \implies s\mathcal{U}_z &= \zeta_x(x) \sigma \mathcal{E}_z \end{aligned} \tag{4.6}$$

Using the new state, the modified Maxwell equations can be rewritten as

$$\partial_y \mathcal{H}_x + \sigma \mathcal{E}_z + \mathcal{U}_z + \zeta_x(x) \epsilon_r \xi_z + s \epsilon_r \mathcal{E}_z = \mathcal{J}_z^{ext} \tag{4.7}$$

$$\partial_y \mathcal{E}_z + \zeta_x(x) \mu_r \mathcal{H}_x + s \mu_r \mathcal{H}_x = \mathcal{K}_x^{ext} \tag{4.8}$$

$$s\mathcal{U}_z - \zeta_x(x) \sigma \mathcal{E}_z = 0 \tag{4.9}$$

Since we are working in the second scenario where the slab is surrounded by vacuum with a relative permittivity $\epsilon_r = 1$ and $\sigma = 0$, we do not have to deal with the third state $\mathcal{U}_z$. In the PML region, which is placed in the vacuum, $\sigma = 0$ and in the area where slab is present, $\zeta_x(x) = 0$. Therefore the term $\frac{\zeta_x(x)}{s} \sigma = 0$ for the entire simulation region and $\left(1 + \frac{\zeta_x(x)}{s}\right) \sigma \mathcal{E}_z$ reduces to $\sigma \mathcal{E}_z$. The equations can be even more simplified by noting that $\epsilon_r = 1$ and $\mu_r = 1$ in the PML area and therefore the term $\zeta_y(y) \epsilon_r \mathcal{E}_z = \zeta_y(y) \mathcal{E}_z$ and $\zeta_y(y) \mu_r \mathcal{H}_x = \zeta_y(y) \mathcal{H}_x$ Using the setting in the scenario two, the modified Maxwell equations can be written as:

$$\partial_y \mathcal{H}_x + \sigma \mathcal{E}_z + \zeta_y(y) \epsilon_r \mathcal{E}_z + s \epsilon_r \mathcal{E}_z = \mathcal{J}_z^{ext} \tag{4.10}$$

$$\partial_y \mathcal{E}_z + \zeta_y(y) \mu_r \mathcal{H}_x + s \mu_r \mathcal{H}_x = \mathcal{K}_x^{ext} \tag{4.11}$$

An interesting observation from the equation 4.10 can be made by putting together the terms involving field value $\mathcal{E}_z$ independent of s which is $(\sigma + \zeta_y)\mathcal{E}_z$. From this grouping, it is seen that ζ_x is essentially the loss in the system just like σ but local only to the PML region. This causes waves to attenuate as soon as the fields hit the PML boundary. This behavior is the same as putting another medium with a loss near the

boundary which will cause reflections. For this reason, a quadratic function is used for the PML function to avoid the presence of a hard boundary.
When discretized, the above equations are written as:

$$\begin{aligned}\hat{Y}h_x + M_\sigma e_z + M_\zeta e_z + sM_\epsilon e_z &= -j_z^{ext}\\ Ye_z + \hat{M}_\zeta h_x + M_\mu \partial_t h_x &= -k_z^{ext}\end{aligned}$$

The above equations can also be written in the matrix form as

$$(D + P + S + Ms)\mathbf{f} = -\mathbf{q},$$

where

$$D = \begin{bmatrix}0 & \hat{Y}\\ Y & 0\end{bmatrix},\ P = \begin{bmatrix}M_\zeta & 0\\ 0 & \hat{M}_\zeta\end{bmatrix},\ S = \begin{bmatrix}M_\sigma & 0\\ 0 & 0\end{bmatrix},\quad \text{and } M = \begin{bmatrix}\epsilon_r & 0\\ 0 & \mu_r\end{bmatrix}$$

On multiplying the above equation by M^{-1}, it is obtained that:

$$\begin{aligned}\left(M^{-1}(D + P + S) + sI\right)\mathbf{f} &= -M^{-1}\mathbf{q}\\ \implies (A + sI)\mathbf{f} &= -\mathbf{b},\end{aligned} \tag{4.12}$$

where $A = M^{-1}(D + P + S)$ and $\mathbf{b} = M^{-1}\mathbf{q}$

Therefore, we obtain the same state space form that we did in the discretization without a PML in chapter 3. With this formulation, we have finally created a discrete truncated model of an open system which is ready for simulation. After the addition of stretched-coordinate PML, the waves inside the PML layer would decay near the boundaries, thus simulating the extension to infinity making our discretized model an open system. Now that we have introduced loss in the system, eigenvalues of the system matrix will be complex, where the imaginary part is the damping and the corresponding eigenvectors are the QNMs. The solution space can now be expanded in terms of QNMs. From our previous discussion, we know that the QNMs corresponding to the frequencies present in the input signal dominate the solution. In the next section, we will develop a mathematical intuition of the concept.

4.3 Dominant QNMs

To see how some modes are more dominant compared to the others for different input frequencies, we expand our solution as a linear combination of the QNMs using the eigenvalue decomposition of A as shown below:

$$\begin{aligned}&(A + sI)\mathbf{u} = \mathbf{b}\\ \implies\ &V(\Lambda + sI)V^{-1}\mathbf{u} = \mathbf{b}\\ \implies\ &\mathbf{u} = V(\Lambda + sI)^{-1}V^{-1}\mathbf{b}\\ \implies\ &\mathbf{u} = V(\Lambda + sI)^{-1}\mathbf{c}\end{aligned}$$

where $\mathbf{c}$ is a column vector.

Multiplying $V = \begin{bmatrix} V_1 & V_2 & \cdots & V_n \end{bmatrix}$ with the column vector $\begin{bmatrix} \frac{1}{\lambda_1+s} & 0 & \cdots & 0 \\ 0 & \frac{1}{\lambda_2+s} & \cdots & 0 \\ \vdots & & \vdots & \\ 0 & 0 & \cdots & \frac{1}{\lambda_N+s} \end{bmatrix} \mathbf{c}$, it is obtained that:

$$\mathbf{u} = \sum_{i=1}^{n} c_i \cdot \frac{1}{\lambda_i + s} V_i$$

From the above equation, it is seen that the solution space of $\mathbf{u}(s)$ is spanned by the eigenvectors of the system matrix A. The scalar coefficient $\frac{1}{\lambda_i+s}$ blows up in magnitude when $\lambda_i \to -s$, and the eigenvector V_i corresponding to such λ_i will have the most dominant contribution towards the solution space.

It has indeed been found experimentally that these dominant eigenmodes exist and for some open resonant system, they can accurately determine the system response for a wide range of inputs. The reduced subset of eigenmodes which are very few in numbers for some systems and their corresponding eigenvalues λ_R (R stands for reduced) is the idea behind creating a reduced order model which can help in reducing the computational cost by several orders of magnitude.

5 Results

In this chapter, we discuss the results obtained for different parameters in our discretized model. We begin by listing down the system parameters that were used in designing the system. The solutions using the analytical approach and the Finite-Difference approach has been shown in section 5.2. The solutions are shown to verify the validity of the discrete model by comparing it with the analytical solution.

In the subsequent sections, we look at how the eigenvalue distribution evolves for different system parameters in order to identify the PML and Quasi-Normal Modes. These eigenvalues will be compared with the scattering poles of the open slab system that were obtained in chapter 2.

To continue with the identification problem, we look at the PML as a lossy medium and compare the PML modes with eigenvectors associated with a lossy slab medium in section 5.5. We finish this chapter by using the identified QNMs to generate the wave-fields and compare it with the solution obtained through the Finite-Difference method.

5.1 System Parameters

In designing the discretized version of the slab system, the following parameters were chosen:

- Central frequency ω of the input pulse
- Length of the simulation region
- Number of discrete points on the system N
- Length of the PML layer on either side
- PML strength coefficient α
- Input pulse location
- Location y_{slab} where the slab medium begins (figure 2.1)
- Slab width
- Permittivity profile of the slab given by the matrix M
- Electrical conductivity σ

While some of the parameters were kept fixed such as the location of the input pulse and the slab medium, others were used as variables to identify the properties of the

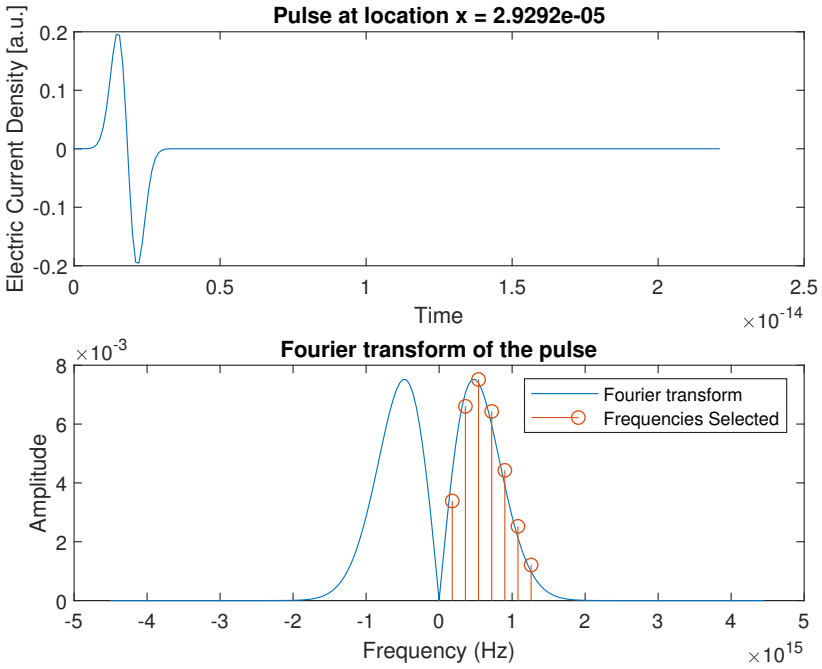

Figure 5.1: Input pulse and Fourier transform

system. The values chosen for this experiment and the rationale behind them has been described below.

Input Pulse:
The first step in the design process is to choose a frequency around which other parameters will be set up. This frequency was chosen in the region of the visible spectrum as $\omega = 4.5 \times 10^{14}$ Hz and corresponding wavelength is $\lambda = \frac{c}{\mu} = 667$ nm. An input pulse with a small bandwidth is generated at time $t = 0$ so that the chosen frequency ω is contained in the Fourier transform of the pulse. The input is chosen to be a derivative of the Gaussian pulse, evaluated at time $t = 0$ as shown in figure 5.1. The normalized central frequency calculated according to chapter 3 is $\omega_{norm} = 37$.

Length of the simulation region:
The length of the simulation space is chosen to be at least twenty times the central wavelength of the spectrum of the input pulse. This length is chosen to be small for faster simulation while making sure that there is sufficient spacing between PML area and the slab system. The length of the system is therefore:

$$L = 13 \ \mu\text{m},$$

The length of the system on the normalized scale is 1.

- From this point the distance will be used in the unit of either the number of discretization points or in mm which is on the normalized scale (section 3) as per convenience.

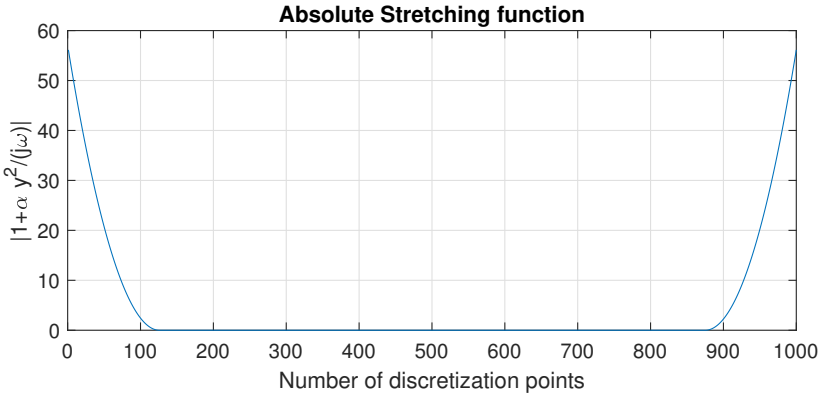

Figure 5.2: Stretching function used for the PML area

Number of sampling points N
The number of sampling points is chosen so that it is significantly greater than the normalized central frequency. In our case, it is chosen to be one thousand unless stated otherwise.

PML Layer:
The length of the PML layer required in a system depends on the geometry and composition of the system and the wavelength of the EM waves used. A small number of grid points is desired for the purpose because the area of interest for the experimentation is the region without the PML layer. After experimenting with different length of the PML, the PML length was chosen to be four times the central wavelength on either side which is 200 discretization points.
In the PML function

$$\chi_y(y, s) = 1 + \frac{\zeta(y)}{j\omega}$$

where,

$$\zeta(y) = \alpha y^2,$$

a scaling factor of $\alpha = 50$ is used to improve the dampening strength of the PML of a given thickness. A plot of the absolute of the stretching function used for initial simulation is shown in figure 5.2.

Input pulse is chosen to be located at a distance of discretization point 350 from the origin (figure 2.1). The slab is placed in the middle of the simulation area starting from the discretization point 500 with a **slab width** of 100. Permittivity of the slab material is chosen as $\epsilon_2 = 4$ (figure 2.1). **Electrical conductivity** is chosen as $\sigma = 0$ for the lossless case and $\sigma = 30$ for the lossy case unless stated otherwise.
We will begin the initial simulation with the values mentioned above.

5.2 Analytical and Finite Difference Solutions

The analytical solution obtained using the above values has been shown in figure 5.3 for the lossy case ($\sigma = 30$) and in figure 5.4 for the lossless case. It is seen that the

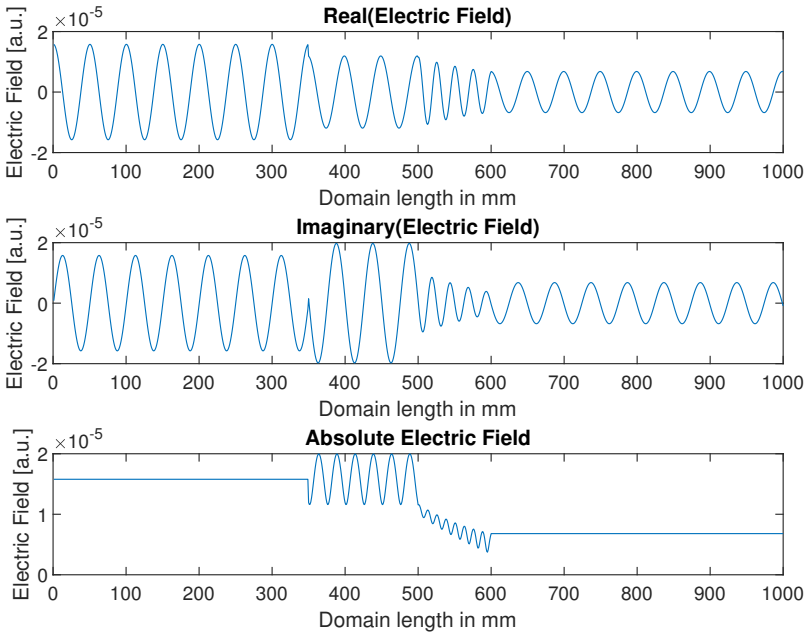

Figure 5.3: Simulated field using the above values for the analytical solution for the lossy case ($\sigma = 0$)

field values attenuate after crossing the slab medium in the lossy case. The scattering poles for the lossless case are shown in fig 5.5.

We will use the solution obtained using the analytical method to validate the output of Finite-Difference solution. Solving for the discretized equation, the electric and magnetic field obtained is plotted in figure 5.6. In the Finite-Difference implementation, our system is surrounded by a perfectly conducting material which is why the field values at the boundaries are zero. The region with the decaying absolute field is the slab area. A PML length of 200 grid points was used for the simulation and as seen in figure 5.6, the field values appear to decay on both sides in the PML region. Similar decay pattern is observed when the waves pass through the slab medium. It is because much like a lossy medium, the PML is a region of higher loss designed to attenuate the outgoing waves with minimal reflections. The real part of the electric field is smooth everywhere except at the source location. Magnetic field suffers discontinuity at the source location as seen in figure 5.6. This discontinuity can be explained by looking at the Maxwell equation which describes the spatial behavior of the magnetic field:

$$\partial_y \mathcal{H}_x + \epsilon_r \partial_t \mathcal{E}_z = -\mathcal{J}_z^{ext}$$

At the source location, $\mathcal{E}_z = 0$ and therefore, $\partial_y \mathcal{H}_x = -\mathcal{J}_z^{ext}$ which is the magnitude of the electric current at the location. Thus,

$$\mathcal{H}_{source_-} - \mathcal{H}_{source_+} > \delta$$

where $\delta > 0$ is a finite number, which explains the discontinuity seen in figure 5.6.

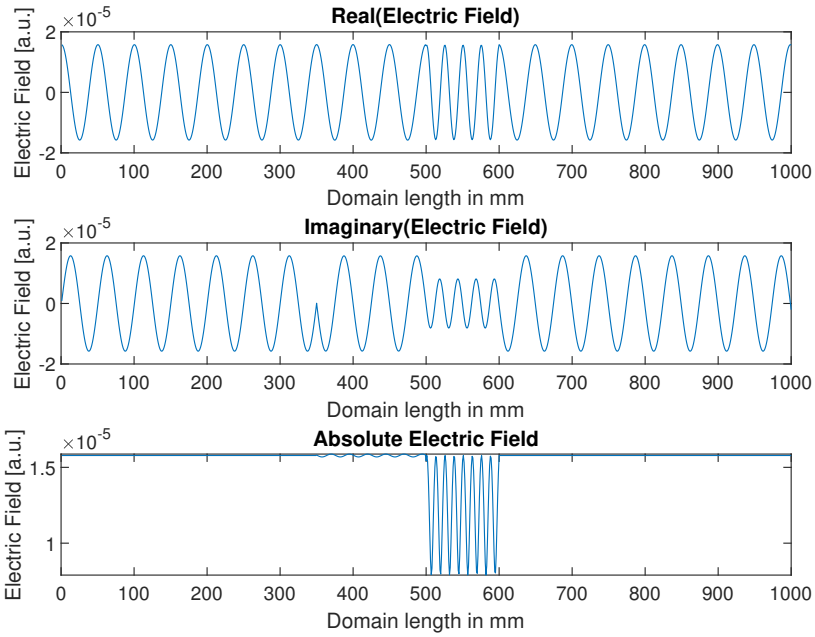

Figure 5.4: Simulated field using the above values for the analytical solution for the lossless case ($\sigma = 0$)

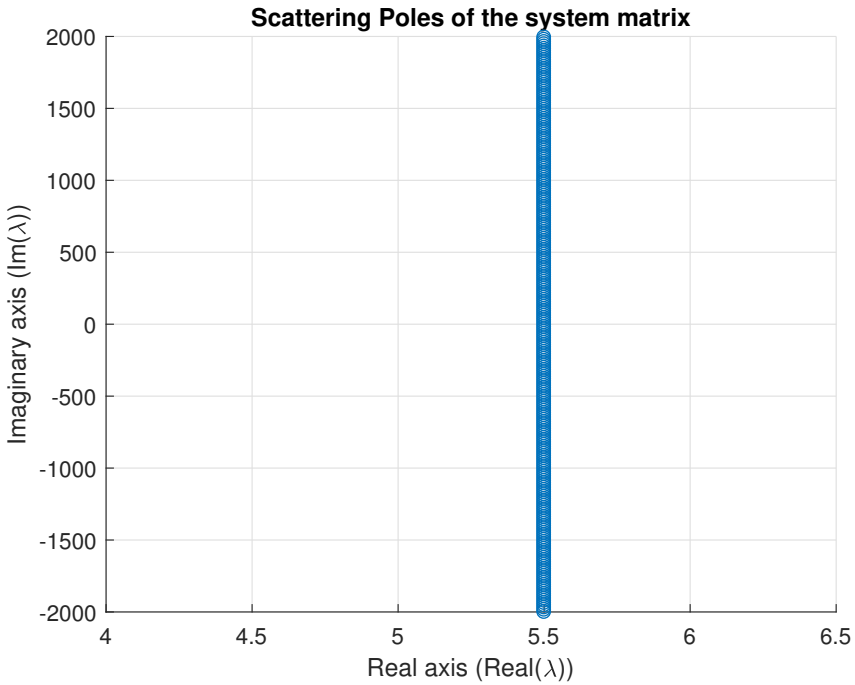

Figure 5.5: Scattering poles of the analytical solution for the lossless case

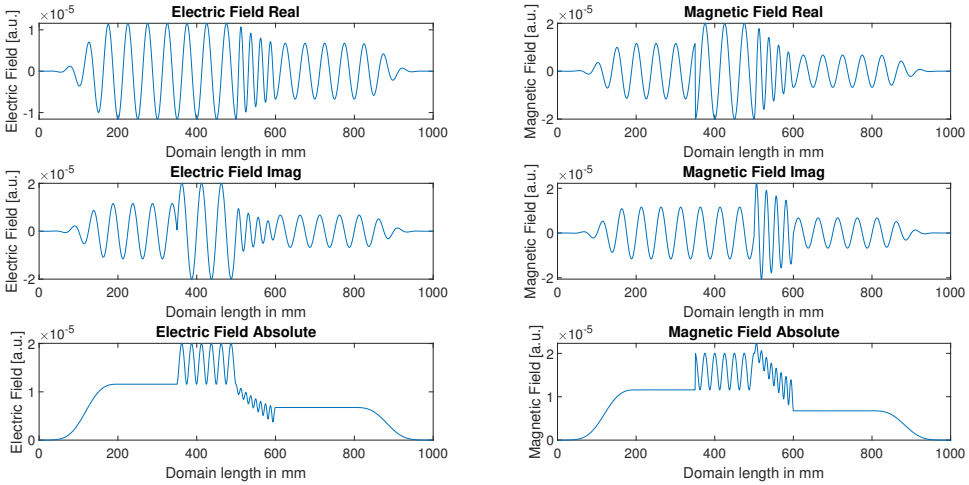

Figure 5.6: Electric and magnetic field in the system with the slab present between grid point $N = 500$ and $N = 600$ having permittivity 4 which is excited by a light wave of frequency 4.5×10^{14}

The wave-field solution, non-differentiability at the source and decay inside the slab medium observed in this case is similar to the analytical solution seen above. Now that we have confirmed the validity of the discrete model, we will proceed to the QNM identification problem in the next section.

5.3 Identifying modes by changing the system parameters

Among all the eigenmodes, we have QNMs, PML modes, and modes that were created due to discretization. In this section, we try to cluster such modes by varying the parameters defining the system. In doing so, we observe the shift in eigenvalue distribution and spread of the corresponding modes. The change in eigenvalue distribution is also compared with the scattering poles of the open system along which the QNMs may lie.

5.3.1 Slab Width

We begin by using the slab width as our variable parameter. One end of the slab is fixed at the discretization point 500 while the other end shifts to the right as slab width is increased. In this analysis, we observe the shift in eigenvalues, their eigenvectors and develop an intuition of a possible structure of the QNMs and PML modes. A plot of eigenvalues of the system matrix for four different slab widths is shown in figure 5.7. It is seen from the figure 5.7a, 5.7b and 5.7c that as the slab widths are increased, eigenvalues which overlap with the scattering poles start shifting towards the imaginary axis while another set of eigenvalues start shifting away from the imaginary axis towards a region of higher damping.

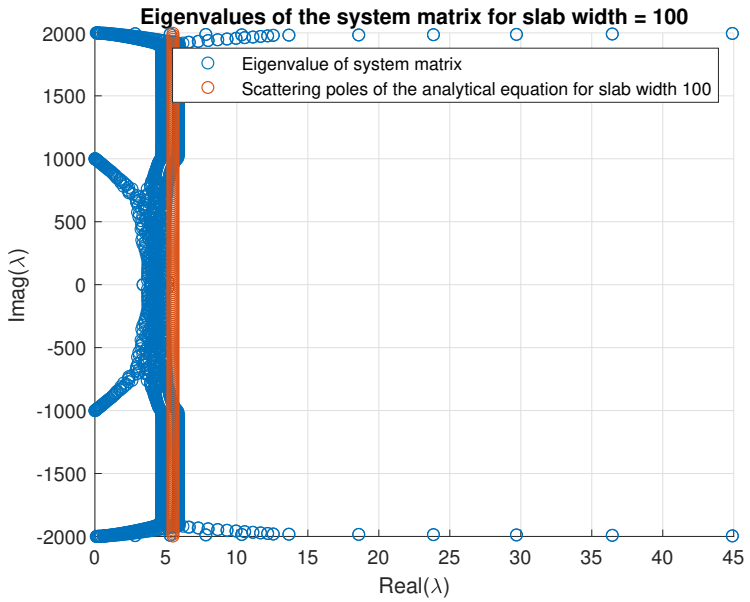

(a) Slab Width 100

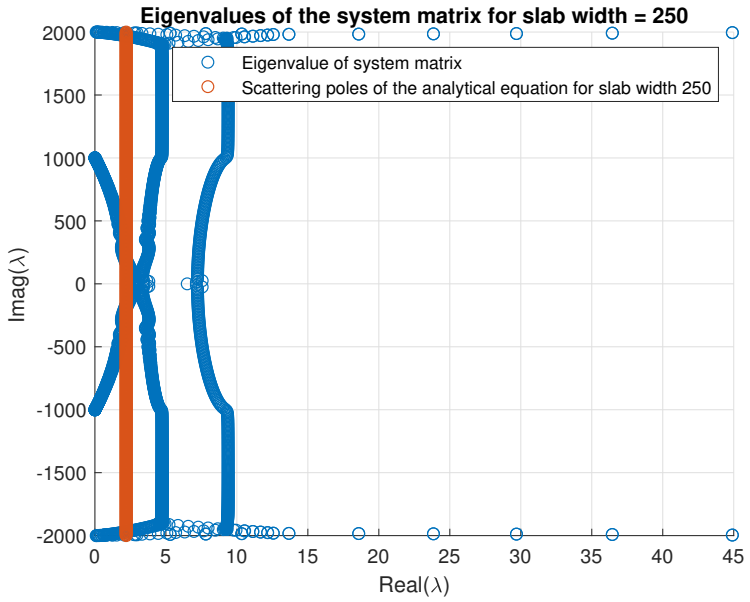

(b) Slab Width 250

To understand what the different bands of the eigenvalues in figure 5.7c mean, we look at the eigenvectors corresponding to different regions of the eigenvalue plot in figure 5.8. The different regions we consider in this case are the three stripes running vertically and the horizontal stripe of sparsely spaced out eigenvalues. A plot of eigenvectors for eigenvalues from these regions is shown in figure 5.8. An eigenvector corresponding to the leftmost stripe overlapping with the scattering poles of the system matrix is shown in figure 5.8a. The eigenvector extending in both the direction is seen to be diverging with distance as expected from a QNM. The wave attenuates near the boundary because

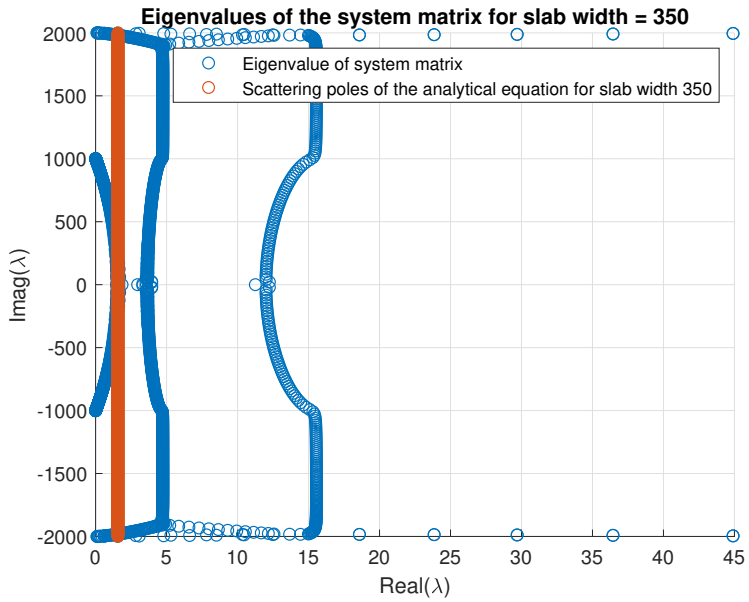

(c) Slab Width 350

Figure 5.7: A plot of scattering poles against the eigenvalues of the system matrix A for different slab widths. As the slab width is varied from the number of discretization points of 100 to 350, it is seen that the QNMs which overlaps with scattering poles starts shifting towards the imaginary axis while the poles due to discretization start shifting away from the imaginary axis towards a region of higher damping. It is thus concluded that the poles which do not change are the PML modes of the system.

of the PML layer. Figure 5.8b and 5.8c are the eigenvectors corresponding to the eigenvalues in the middle and the right stripe of the eigenvalue plot respectively. These vectors show waves travelling in left and right directions from the point the slab begins and ends respectively. Again, as expected, as the slab width is increased, the rightmost stripe will move to a region of higher damping because the wave travelling towards the right is travelling a larger distance in the lossy medium than the waves travelling to the left. This explains why the second stripe stayed static while the rightmost stripe moved as slab width was increased. Finally, the conclusion that can be drawn after looking at the eigenvector in figure 5.8d is that they correspond to the PML modes. These eigenvectors are localized in the PML area and the corresponding eigenvalues are unaffected by the shift in slab width. From these results, we also claim that the modes corresponding to the eigenvalues overlapping with the scattering poles are the QNMs of the system. Further analysis of the PML modes will be carried out by looking at the shift in eigenvalues by changing the PML parameters which will be discussed later.

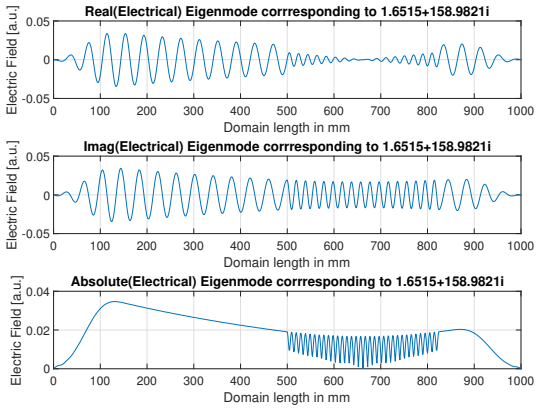

(a) The eigenvector corresponding to the eigenvalue overlapping with the scattering poles of the slab system. They are the QNMs of the discretized system.

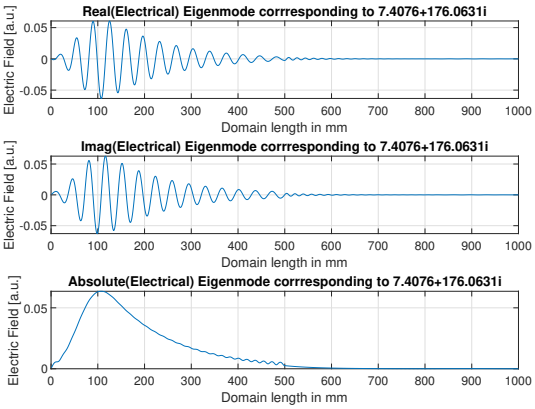

(b) Eigenvector from the middle stripe shows wave travelling in the left direction from the slab location. These eigenvectors are unaffected by the increase in slab width

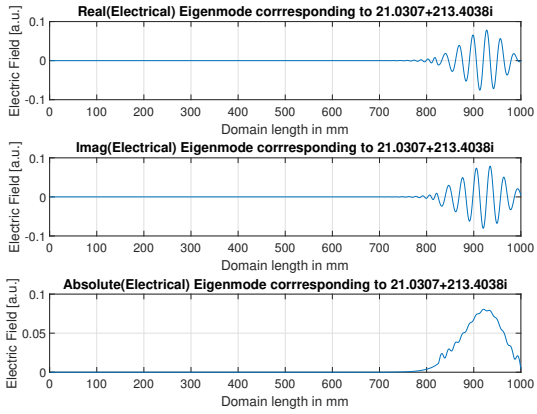

(c) Eigenvector showing wave travelling to the right. As slab width is increased in the right direction, the eigenvalues shift towards the right in a a region of higher damping.

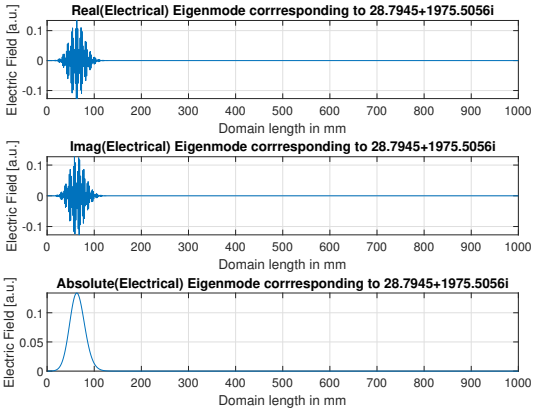

(d) The eigenvector is one of the PML modes of the system. These eigenvectors are localized in the PML region.

Figure 5.8: Eigenvectors corresponding to some of the eigenvalues calculated for the slab width of 350mm. The top-left eigenvector is for the eigenvalue $7{+}176i$ which is the middle stripe in figure 5.7c. The top-right corresponds to the eigenvalue from the right stripe and the bottom-left is from the stripe coinciding with the scattering poles of the system. The bottom-right eigenvectors is the suspected PML mode and corresponds to the sparsely distributed eigenvalue stripe on the top ($28{+}1975i$).

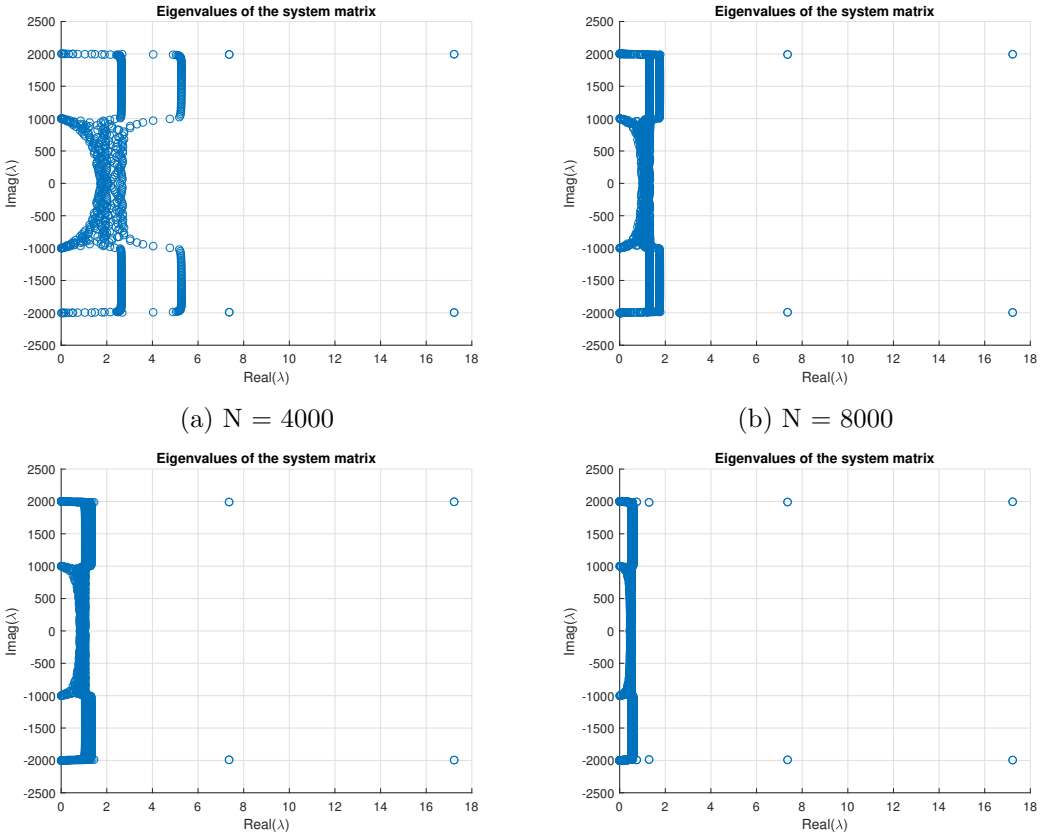

(a) N = 4000

(b) N = 8000

(c) N = 1000

(d) N = 2000

Figure 5.9: A plot of eigenvalues of the system matrix for the different number of sampling points N. The density of eigenvalues around the QNM region increase much more than those in the region of PML modes.

5.3.2 Number of discretization points N

Now that we have seen the effect of changing slab width on the eigenvalues of the system, we will look at the impact of the number of sampling points. We use $N = 400, 800, 1000$ and 2000 to draw out the comparison. From previous results, we have claimed that the horizontal stripe of sparsely distributed eigenvalues is the region of PML while the scattering poles overlapping with the rest are QNMs. It is expected that by increasing N, the discrete model will approximate the true solution which can be concluded from figure 5.9. It is seen that increasing N creates more eigenvalues in the region of QNMs than in the region of PML modes.

5.4 Understanding effect of PML Length

In the previous sections, we saw the change in eigenvalue distribution and the corresponding eigenvectors as the system parameters were varied. We also managed to obtain an idea of the structure of eigenvectors corresponding to the PML modes. In this section, we see how changing the PML parameters can affect the spectrum and we study the eigenvectors to further our claim from the previous sections on the clustering of different regions. In figure 5.10, there are four different plots corresponding to different PML lengths. Increasing the PML length does not change the scattering poles or the overlapping eigenvalues of the system matrix A which are the QNMs of the system. The stripe moving to the right is because of the same reason as was seen for figure 5.8. The eigenvectors with waves travelling in the left and right direction begin to fall inside the PML region as PML length is increased. These eigenvalues get separated from the rest as the more area of the system falls into the region of higher damping.

It can be thus concluded that the horizontal stripe of eigenvalues correspond to the PML modes because only these eigenvalues are affected on increasing the PML length. From the previous section, we know that the corresponding eigenvectors are localized in the PML region. These modes separate once the parameters associated with the property begins to dominate over other parameters of the system. This is true for a PML because it is required to decay the wave in a small region by design. Thus, the corresponding eigenvalues can be found by locating the group of eigenvalues separate from the rest and whose eigenvectors are localized in the PML region.

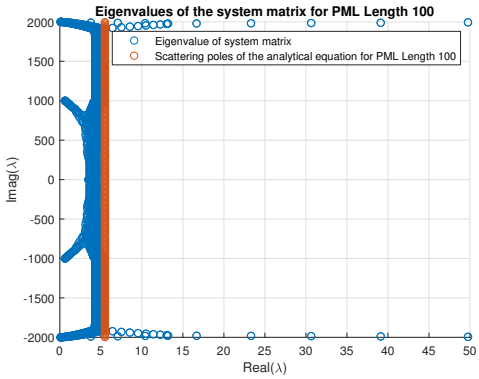

(a) PML length = 100 discretization points.

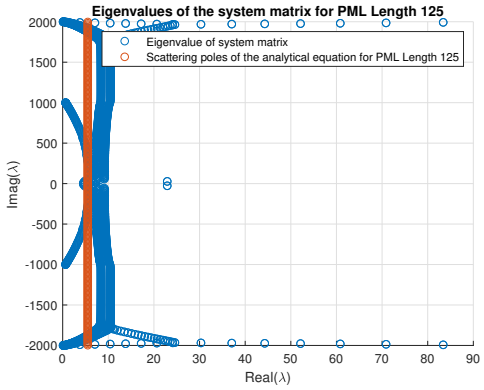

(b) PML length = 125 discretization points.

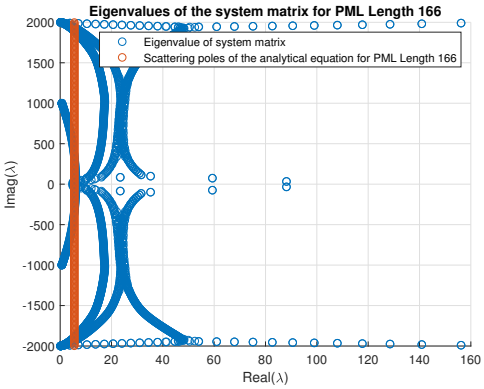

(c) PML length = 166 discretization points.

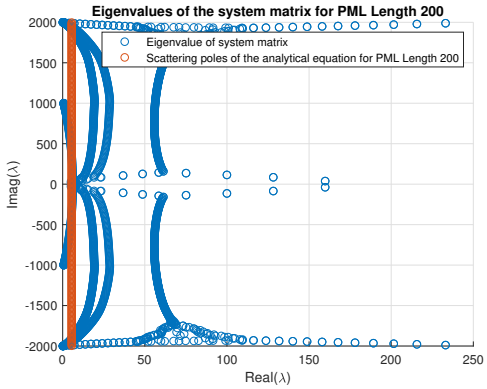

(d) PML length = 200 discretization points

Figure 5.10: Eigenvalue plot of the system matrix when using different lengths for the PML area. It is observed that approximation of scattering poles by the system matrix is limited by the length of the PML.

5.5 Visual Inspection of Eigenmodes

We continue from the last section by reflecting on some of the conclusions that were drawn based on our observations. In this section we will look at the spread of eigenvectors in different regions of the eigenvalue plot. We begin with a visual inspection of the eigenmodes for different eigenvalues to see how PML modes look different from the QNMs. Figure 5.11 shows a plot of eigenvalues and the eigenvectors for a selection of eigenvalues. The colorbar represents the extent of energy that is present in the eigenvector for the entire system excluding the PML area.

The eigenvalues on the horizontal axis on the top and the bottom correspond to the PML modes. These eigenvalues have eigenvectors localized in the PML region and therefore have lower energy compared to the other region in the plot which can be seen from the eigenvector plot in the same figure. One characteristic of these modes is that they are more spaced out than the relatively denser eigenvalues of the system.

We will also see the effect of electrical conductivity σ on the eigenvalue spectrum. Since PML behaves as a lossy medium, we expect that the eigenvalues and eigenvectors corresponding to the slab medium which is affected by σ should have a structure similar to the PML modes. For further validation of the conclusions drawn upon the characteristics associated with the PML modes, we continue the analysis in the slab region using a high σ. We look at the shift in eigenvalues for different σ's and to make the plot readable, we use a smaller $N = 400$. From figure 5.12, it can be verified, that only a portion of the eigenvalue distribution is changing when the parameter σ is varied. These are the same eigenvalues corresponding to which the eigenvectors are localized in the lossy slab area as seen in figure 5.13. It can also be seen that these eigenvalues are much less dense than other groups in the eigenvalue plot (figure 5.12) much like how it was observed for the PML modes.

After looking at similar behavior exhibited by the PML modes and the lossy slab modes (modes localized in the slab medium), we have concluded that modes in a lossy region like a PML will be localized and the corresponding eigenvalues will be sparsely populated separated from the rest of the modes. However, this kind of localized behavior is seen only when the loss in the region is significantly greater than in other regions. This makes sense because if the parameters pertaining to separate regions are not considerably different, there will not be a significant difference in the behavior of those regions. However, this is not a problem as far as the identification of the PML modes are concerned because the PML is designed in such a way that the attenuation in that region is much more than the rest of the system so that the wave decays exponentially in the small PML area. Therefore, it can be said that the PML modes can be identified by looking at the sparsely spaced set of eigenvalues and their corresponding eigenmodes which will be localized in the PML area.

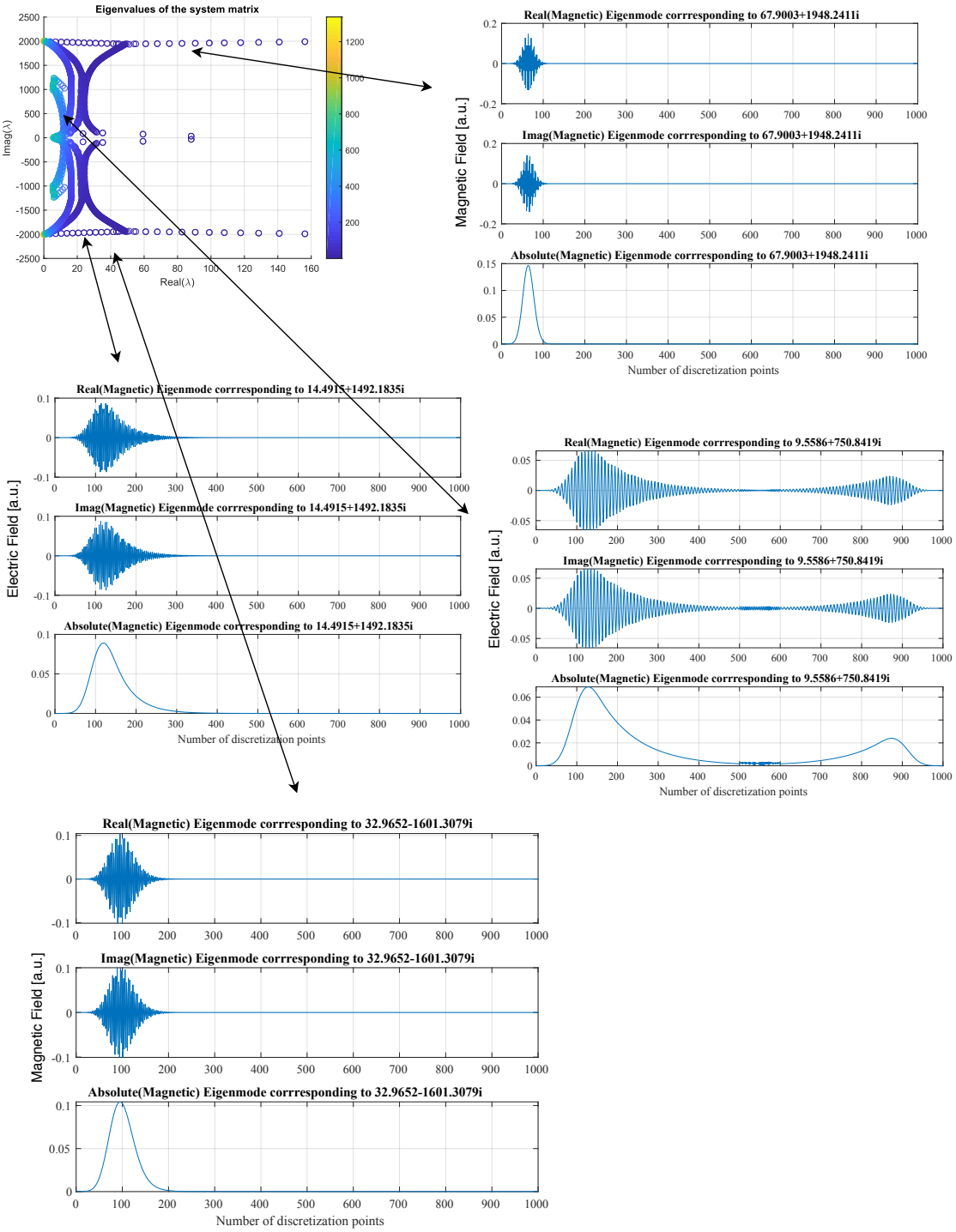

Figure 5.11: Eigenvectors corresponding to different eigenvalues. The top-right corner is the one corresponding to one of the PML modes while the center-right is a mode corresponding the eigenvalue overlapping with the analytical scattering pole. The colorbar on the eigenvalue plot represents the energy in the signal present in the non-PML area. It is interesting to see that while the eigenvectors for the QNMs are spread over the entire region (center right), the PML modes are localized in the PML region(center right).

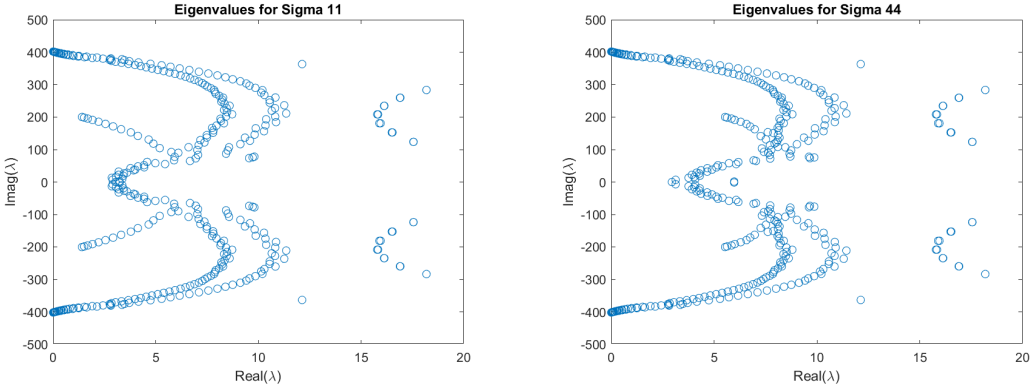

(a) Sigma = 11

(b) Sigma = 44

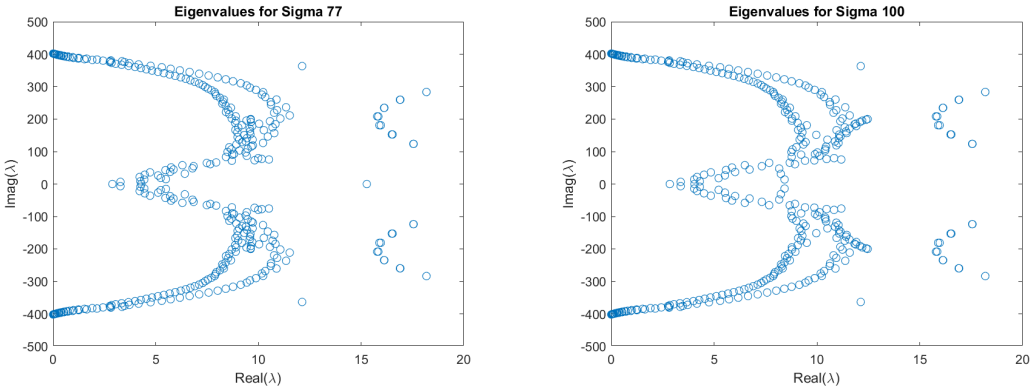

(c) Sigma = 77

(d) Sigma = 100

Figure 5.12: A plot of real vs imaginary part of eigenvalues for different sigmas. It is seen that only the eigenvalues related to the region of the slab are shifting with changing sigmas

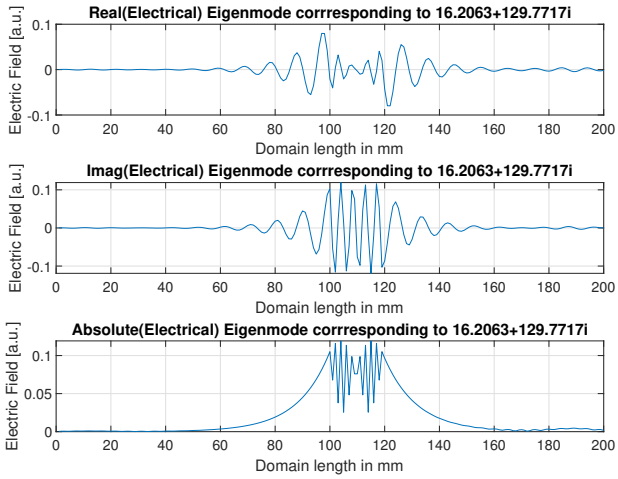

Figure 5.13: Eiegnvector corresponding to the eigenvalue in the slab area. For a large σ, the eigenvalues separate and the corresponding eigenvectors are localized in the slab region.

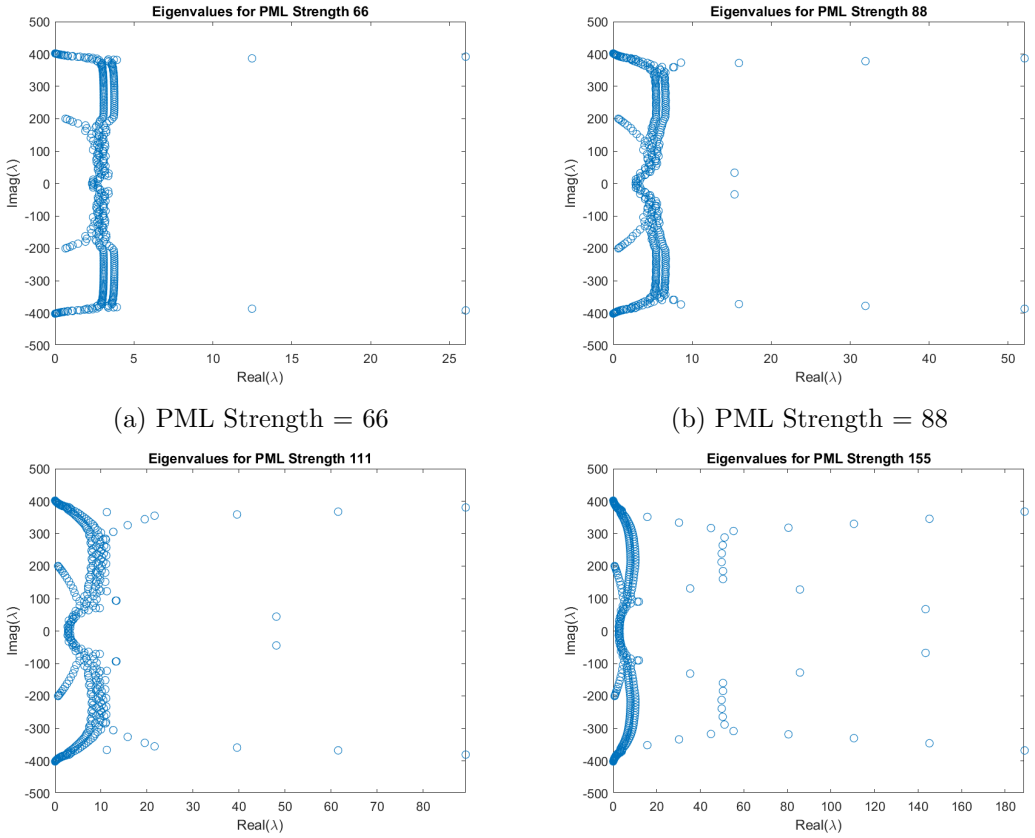

(a) PML Strength = 66

(b) PML Strength = 88

(c) PML Strength = 111

(d) PML Strength = 155

Figure 5.14: A plot of real vs imaginary part of eigenvalues for different PML strength α. Some of the eigenvalues on the horizontal stripe correspond to the PML modes while some to the slab area.

We perform a similar experiment with the PML parameter α for $N = 400$ and $\sigma = 300$ where we observe the shift in eigenvalues. In this experiment, we expect to have both the PML modes and the modes associated with the slab medium to separate, since these regions have significantly greater loss than the other regions in the system. It is seen that initially (figure 5.14a) when all the values are comparable, there is no clear distinction between different areas and there are still reflections from the boundary. The eigenvalues on the top and bottom correspond to the slab region and the eigenvector look similar to figure 5.13. As PML strength is increased, more eigenvalues start separating. To verify that the eigenvalues separating are indeed the PML modes, the corresponding eigenvector of one of the eigenvalues from figure 5.14d is observed in figure 5.15 which is found to be localized in the PML area.

With this result, we finish our study on the parameters of the system. We have now clustered different regions of the eigenvalue distribution and now we can test whether the QNM region by itself is sufficient to get the solution or not in the next section.

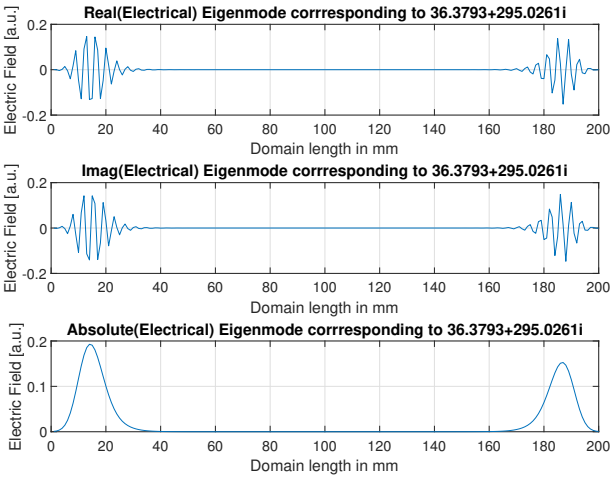

Figure 5.15: Eigenvector corresponding to one of the eigenvalues from the figure 5.14c.

5.6 Some results on selecting bands of eigenmodes

In the previous sections, we identified the set of eigenvalues whose eigenvectors are the QNMs and managed to find a structure for the PML modes. In this section, we see how good the eigenmodes which were identified as QNMs are in reconstructing the original solution. For this purpose, we will use four different bands of eigenvalues:

- Both end of the spectrum excluding the horizontal stripe of PML modes (Eigenvalues with imaginary part ranging from -1000 to 1000)
- Eigenvalues with the positive imaginary part
- Eigenvalues with the negative imaginary part
- Entire spectrum of eigenvalues excluding the region around the frequency of the input pulse

A plot of results obtained through Finite Difference for the frequency $\omega = 4.5 \times 10^{14}$ has been shown in figure 5.6 for the comparison purpose.

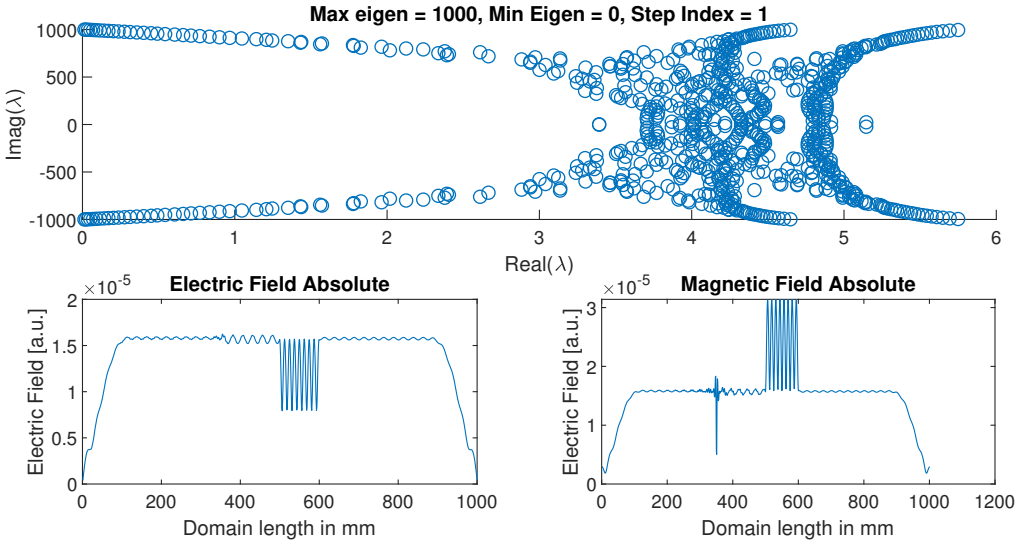

Figure 5.16: Electric field and Magnetic field obtained when both the positive and negative eigenvalues are used for the calculation.

Through previous experiments, it was seen that the eigenvalues of interest are in the low-frequency area and the sparsely populated modes on the top and the bottom are the PML modes. To see if it is indeed true or not, we try to get the solution using only those modes, the corresponding eigenvalues of which has imaginary values between -1000 and 1000. The obtained solution in figure 5.16 is a close approximation to the true solution, thereby highlighting the role of QNMs.

While the limited number of eigenvalues is enough to construct a solution as seen in figure 5.16, what will happen if either only the positive or negative eigenvalues

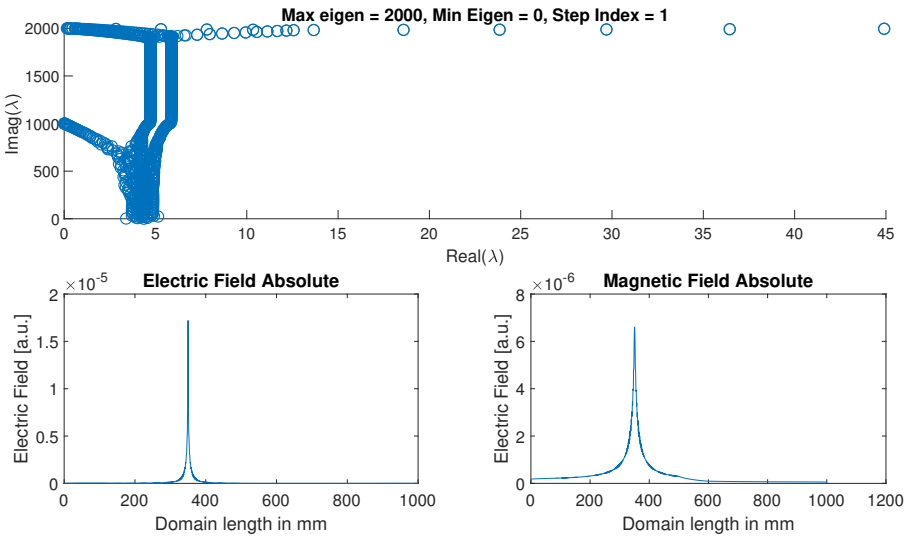

Figure 5.17: When only the positive eigenmodes are used, the solution obtained does not compare well with the Finite Difference solution at all. This is because the dominant eigenmode in our case lies in the range 0 to -30.

are used? From the previous mathematical analysis, it has been established that the dominant eigenmodes are those whose eigenvalue $\lambda \to -j\omega$, where ω is a frequency in the bandwidth of the input pulse. If only the positive eigenvalues are being used, it should not be possible to get an approximate solution, which can be seen from figure 5.17. Here, the entire range of modes whose imaginary part of the eigenvalue is greater than zero is used.

Next comes the case where only the eigenmodes with negative eigenvalues are used. As expected, although the solution is not as good as using both ends of the spectrum, it is a good approximation of the original solution (figure 5.18).

Now, on to the case, where the entire spectrum of eigenvalues is used except a very narrow band which contains the QNM corresponding to the frequency of the input pulse. It is not surprising to see from the figure 5.19, that although almost the entire spectrum is being used, the solution is still nowhere close to the actual one. It emphasizes on the importance of dominant QNMs and how a small set of modes represent the entire resonant system.

From these results, it can be seen it is possible to obtain a reduced-order model for the system. Although, the slab system discussed in this paper is easy to implement and solve for analytically, it does not have a finite set of scattering poles which makes it difficult to use for analysis in the subject at hand. Systems such as gold film used as nano-resonators have a very small set of frequencies which acts as QNMs and for such system, it is possible to significantly reduce the order.

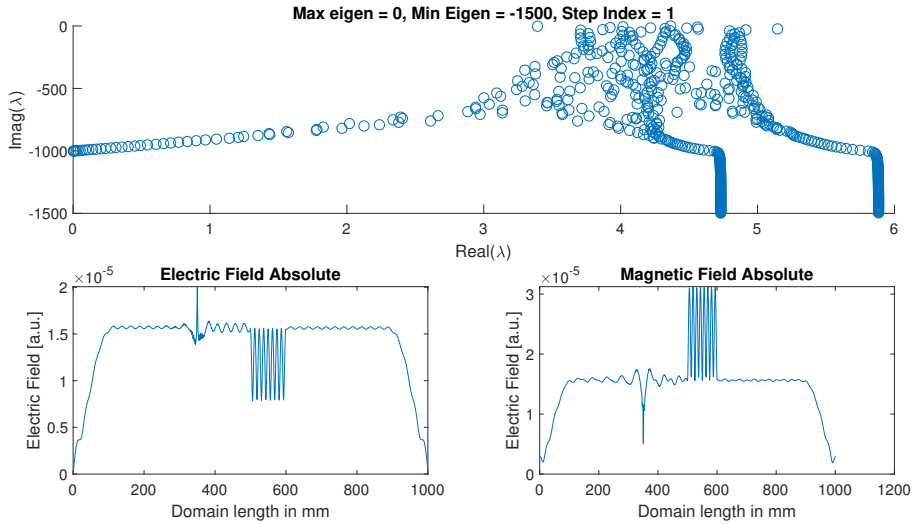

Figure 5.18: When only the negative eigenmodes are used, the solution is much closer to the Finite Difference solution, although still not as good as when both the positive and negative modes are used.

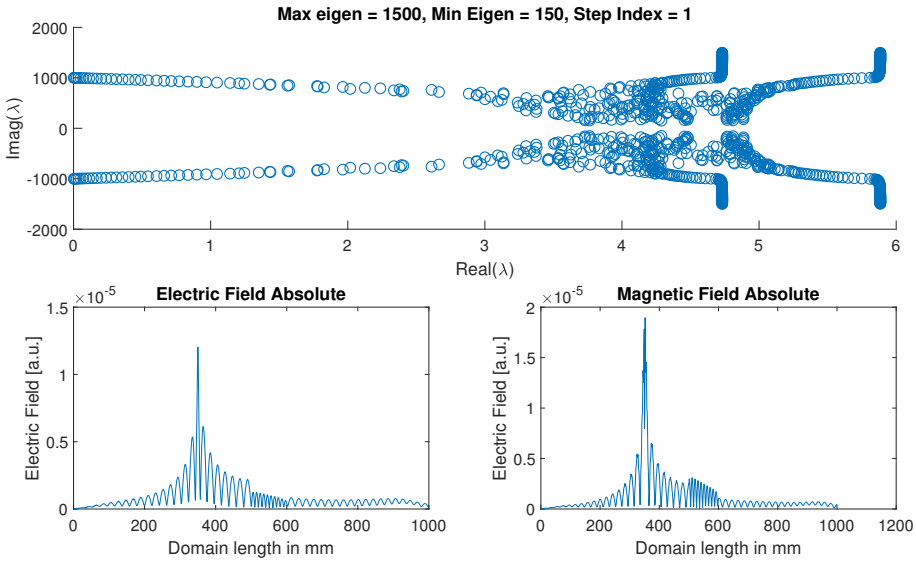

Figure 5.19: When the dominant eigenmodes whose imaginary values lie around the region -150 to 150 are removed, then no matter how many eigenvalues are chosen, a solution close to the one obtained through Finite Difference method is not reached.

6 Conclusion

The behavior of the system governed by Maxwell's equations was observed in this report for different parameter values. It was seen that changing the system parameters only affected a certain set of eigenvalues specific to the region linked with those parameters. Also, the eigenvectors corresponding to these eigenvalues were concentrated in specific regions instead of being spread out to the whole space. This is an important result when localized eigenvectors are desired for specific applications.

The behavior of the PML region was established to be similar to the region of the lossy medium. In the process, the structure of the associated mode was found to be localized in the respective region of the loss. It was further observed that when the PML strength or the loss (σ when looking at the slab region) is not high, there is no visible separation between the modes and the eigenvectors are not localized. Changing the loss parameters shifts the entire range of eigenvalues until a point where eigenvectors start getting localized to the region and further increasing the loss results in a shift in only the associated eigenvalues. When it comes to the identification of the PML modes, the PML parameters is chosen to be higher in magnitude compared to the parameters of other regions. This facilitates the attenuation of the outgoing waves in a small region. Therefore, it can be concluded that PML modes will be localized and separated from the rest of the modes in a practical simulation environment.

Furthermore, it was observed that reconstructing the solution using only a part of the entire spectrum of eigenvalues were possible only when the eigenmode corresponding to the input frequency was considered which further verified the validity of dominant Quasi-Normal Modes. Though the system considered here is geometrically simple, it has an infinite set of scattering poles parallel to the imaginary axis and therefore is not suitable for simulations related to the QNMs. A more complicated system possessing only a small set of scattering poles will be a much better choice and can reveal more appealing results in the identification of QNMs.

Future work on this thesis may involve exploiting the sparsely distributed nature of the PML modes. A suitable filter can also be used because a notion of the structure of the PML modes have been developed in the sense that they are localized in the PML region.

Bibliography

[1] Jean-Pierre Berenger. "A perfectly matched layer for the absorption of electromagnetic waves". In: *Journal of computational physics* 114.2 (1994), pp. 185–200.

[2] Weng Cho Chew and William H Weedon. "A 3D perfectly matched medium from modified Maxwell's equations with stretched coordinates". In: *Microwave and optical technology letters* 7.13 (1994), pp. 599–604.

[3] ESC Ching et al. "Waves in open systems: eigenfunction expansions". In: *arXiv preprint gr-qc/9904017* (1999).

[4] Vladimir Druskin, Rob Remis, and Mikhail Zaslavsky. "An extended Krylov subspace model-order reduction technique to simulate wave propagation in unbounded domains". In: *Journal of Computational Physics* 272 (2014), pp. 608–618. ISSN: 0021-9991. DOI: https://doi.org/10.1016/j.jcp.2014.04.051. URL: http://www.sciencedirect.com/science/article/pii/S0021999114003271.

[5] Semyon Dyatlov and Maciej Zworski. *Mathematical theory of scattering resonances*. American Mathematical Society, 2019.

[6] Rémi Faggiani et al. "Modal Analysis of the Ultrafast Dynamics of Optical Nanoresonators". English. In: *ACS Photonics* 4.4 (Apr. 2017), pp. 897–904. ISSN: 2330-4022. DOI: 10.1021/acsphotonics.6b00992.

[7] Steven G Johnson. "Notes on perfectly matched layers (PMLs)". In: *Lecture notes, Massachusetts Institute of Technology, Massachusetts* 29 (2008).

[8] Philippe Lalanne et al. "Light Interaction with Photonic and Plasmonic Resonances". In: *Laser & Photonics Review* 12 (May 2018), p. 1700113. DOI: 10.1002/lpor.201700113. arXiv: 1705.02433 [physics.optics].

[9] C. Sauvan et al. "Theory of the Spontaneous Optical Emission of Nanosize Photonic and Plasmon Resonators". In: *Phys. Rev. Lett.* 110 (23 June 2013), p. 237401. DOI: 10.1103/PhysRevLett.110.237401. URL: https://link.aps.org/doi/10.1103/PhysRevLett.110.237401.

[10] Dipl-Ing Dr Joachim Schöberl and Maria Rechberger. "Numerical Methods for the Simulation of Acoustic Resonances". In: ().

[11] Michael H Tooley. *Electronic circuits: fundamentals and applications, Newnes*. 2006.

[12] MD Verweij, PM van den Berg, and H Blok. *Electromagnetic Waves: An Introductory Course*. DUP Blue Print, 2001.

[13] Jörn Zimmerling et al. "Model order reduction of electromagnetic wavefields in open domains". In: *GEOPHYSICS* 83 (Dec. 2017), pp. 1–38. DOI: 10.1190/geo2017-0507.1.